Double Layer Formation and Cation Pseudo-Intercalation Supercapacitor Carbon Nanotube Composite Electrodes with Enhanced Electrochemical Performances

by

Yverick Pascal Rangom

A thesis

presented to the University of Waterloo

in fulfillment of the

thesis requirement for the degree of

Master of Applied Science

in

Electrical and Computer Engineering – Nanotechnology

Waterloo, Ontario, Canada, 2014

AUTHOR'S DECLARATION

I hereby declare that I am the sole author of this thesis. This is a true copy of the thesis, including any required final revisions, as accepted by my examiners.

I understand that my thesis may be made electronically available to the public.

_____

Yverick Pascal Rangom

ABSTRACT

Among electrochemical energy storage solutions, redox-free supercapacitors exhibit the highest power densities and best cycle life, easily reaching over one million cycles. Despite these attributes, Li-ion batteries are preferred for most applications, especially in the much sought after electric vehicle applications. The reason is the lower energy density of the former compared to the latter. Nevertheless supercapacitor technology remains complementary to batteries in many ways. The excellent cycling performance of non-redox supercapacitors derives directly from their highly reversible charge storage mechanisms. Currently, efforts in the scientific community are being put into addressing i) low energy density, ii) compromised electronic and ionic charge transport, iii) small potential window for devices using aqueous electrolyte. All three research areas are fundamental to supercapacitor systems, however increased charge transport carries the greatest promises in terms of future device developments. The original research, presented in chapters 3 and 4 of this thesis, focuses on the characterization and optimization of electronic and ionic conduction phenomena in supercapacitors relying on double layer formation and pseudo-intercalation charge storage mechanisms.

Chapter 3 features a novel carbon architecture that is both mesoporous and highly conductive based on naturally occurring carbon nanotube (CNT) mesh structure. The structure favors both mostly un-impaired ion movement and excellent electronic conductivity. Filtering these self-standing films from chlorosulfonic acid dispersions presents the critical advantage of not permanently functionalizing the carbon and fully preserves its electronic conductivity. The pristine condition of carbons after filtration is confirmed by fourier transform infrared (FTIR) spectroscopy based on comparison with the material before exposure to chlorosulfonic super-acid. The films were then mated to current collectors with

different surface roughness and chemistries exposing the carbon/metal interface as a critical bottleneck limiting ultimate electronic conductivity. Surface morphologies were characterized at the micro- and nano-size with contact profilometer and atomic force microscopy (AFM) respectively. Surface oxidation was investigated through x-ray photoelectron spectroscopy (XPS) characterization. The study showed that surface morphology played the most important role in facilitating electron transfer between solids while the surface chemical composition was less of a factor.

In Chapter 4, a 2-D Ti_2C Mxene-CNT composite electrode was produced using a similar dispersion and filtration technique as in Chapter 3. The good chemical stability of Mxene allowed for dispersion in superacid with no effect on its inter-planar distances. That was verified by comparing spectra before and after exposure to the super-acid. Mxene phase electrodes have been demonstrated to have extremely high specific capacitance with regards to their specific surface area thanks to a charge storage mechanism that involves cations being stored in-between sheets in a pseudo-intercalation mechanism. Capacitance values around 100 F/g at 1 A/g of specific current are obtained with a total specific surface of less than 30 m^2/g. The composite CNT-Ti_2C electrode show significantly improved performance over the original Mxene material when cycled alone; 100 F/g capacitance is maintained at more than 100 A/g. Composite films made from an exfoliated and sonicated Mxene phase have double the volumetric energy than non-exfoliated CNT-Ti_2C thanks to more dense packing of materials. Electrochemical Impedance Spectroscopy (EIS) Nyquist plots reveal a value for current collector interfacial impedance that is smaller than that of the CNT-films from Chapter 3. This result demonstrates the relevance of physical engineering of contacts, even in a situation where only conductive materials are used, showcasing the decisive advantage of the 2-D morphology of Mxene over the 1-D tubular morphology of CNTs in the task of producing greater effective contact area.

Acknowledgements

I would like to thank Professor Linda Nazar for providing a fitting environment where original research could be freely conducted. The excellent conditions I benefitted from throughout my time here Prof. Nazar's lab were instrumental in the production of this thesis.

I would like to thank Professor Shirley Tang for accepting me as a member of her group and for her guidance.

The students and post-doctoral fellows in both Prof. Nazar and Prof. Tang groups have been great people to work with throughout the years. Dr. Mayhar Mazloumi, Samaneh Shadmehr, Dr. Xiao Liang, Dr. David Donkor, and Xiguang Gao are especially acknowledged for actively helping my research progress.

Finally I would like to recognize Professor Bo Cui for making this endeavour in UW's E.C.E. department possible.

Table of Contents

List of figures

List of tables

Glossary

AC	Activated Carbon
AC	Alternative Current
AFM	Atomic Force Microscopy
BET	Brunauer Emmett Teller (refers to instrument)
CNT	Carbon Nanotube
CSA	Chlorosulfonic Acid
CV	Cyclic Voltammetry
CVD	Chemical Vapour Deposition
DC	Direct Current
DI	De-Ionized water
DMSO	Dimethyl Sulfoxide
EDLC	Electrochemical Double Layer Capacitor
EES	Electrical Energy Storage
EIS	Electrochemical Impedance Spectroscopy
ESR	Equivalent Series Resistance
FTIR	Fourier Transform Infrared spectroscopy
GS	Galvanostatic cycling
HF	Hydrofluoric acid
Li	Lithium
LTO	Lithium Titanate Oxide
MWNT	Multi-Walled carbon Nanotube
PANI	Polyaniline
PC	Porous Carbon
PPy	Polypyrrole
SEM	Scanning Electron Microscopy
SWNT	Single Walled carbon Nanotube

TGA	Thermal Gravimetric Analysis
XPS	X-ray Photoelectron Spectroscopy
XRD	X-Ray Diffraction

CHAPTER 1 – INTRODUCTION

1.1 Overview of supercapacitors

Our globalized human society is completely reliant on fossil fuels. Non-renewable energy is used in vast quantities for heating, electricity generation, transportation and, crucially, for food production in the form of fertilizers, pesticides and to power farm machinery. At the beginning of the 21st century strong interest for the electrification of transportation appeared and development of electric energy storage has started to ramp-up in a combine effort of increasing energy use efficiency, limiting CO_2 emission and conserving the fossil resources needed for our subsistence[1]. Transportation is one of the largest consumers of oil; fortunately advancements in electrical energy storage (EES) technology are on the verge of enabling us to taking it away from that sole energy source.

In most EES applications, batteries are the primary medium for storage because of their inherently superior energy density, but supercapacitor technology perfectly complements batteries in every other area: long cycle life, high-power delivery, high-frequency response and energy efficiency at high specific currents. All of these attributes derived from the fast response of the simple capacitive charge storage mechanisms channelled through ever more advanced electrode designs favoring facile ion and electron movements. Non-redox charge storage mechanism in supercapacitors, whether it be double-layer charge formation or ion-intercalation phenomena, is in principle only restricted by ion and electron mobility from electrolyte viscosity, electrical resistance and particle inertia. So, as the high energy density of batteries allows a vehicle to travel far, high power and high energy efficiency under high currents enables it to accelerate strongly, operate with low heat generation and be recharged fast and efficiently. Therefore the next generation EES solutions able to meet the energy and power demands found in automotive applications rely on today's understanding and development of charge

transport phenomena in supercapacitor technologies. Transportation applications are taking a defining role in EES research and developments around the world[1].

1.1.1 Basic concepts

Supercapacitors, also known as electrochemical capacitors, are rechargeable electric storage devices like secondary (rechargeable) batteries. Like secondary batteries, supercapacitors are used in applications where electrical power is needed by an external load. Traditionally supercapacitors are associated with applications necessitating short power bursts whereas batteries are mostly used to energize devices for long periods of time[2]. Nearly all commercial supercapacitors store charges on their electrode surfaces while batteries are able to store much more charges in the bulk of their electrode materials. Part of the work presented in this thesis is one of the earliest efforts aimed at extending supercapacitor applications beyond high-power capabilities and into high-frequency response capable charge storage solutions (120 Hz and beyond). Supercapacitors are ideally envisioned to be used in conjunction with batteries in complex EES systems that take advantage of the strengths of both technologies.

Supercapacitors share a similar basic architecture to secondary batteries: a cell consists of two electrodes placed in an electrolyte. Cells may be asymmetrical with one electrode designed to store cations and the other intended to store anions only, or cells may also have identical electrodes able to store anions and cations indifferently. Electrostatic forces govern the storage of electrical energy in redox-free supercapacitors. On the other hand, redox pseudo-capacitors store energy through fast, repetitive surface redox reactions. Therefore, state-of-charge is directly related to electrode potential unlike batteries that present potential plateaus during charge and discharge. Storing charges in a double layer leads to cell potentials that decay exponentially with the amount of charges left on the electrodes.

Materials used to make electrodes must be good electric conductors and present a large surface area contacting the electrolyte. The electrolyte may be a liquid or a solid that is conductor to ions but not to electrons. In the case of cells using liquid electrolytes, electrically insulating porous separators keep electrodes apart[3].

Basic evaluation of supercapacitor electrodes involves measurements of capacitance, series resistance and frequency response. Capacitance figures are routinely presented as a function of weight, volume, area, cycle number, specific current and sweep rate. Capacitance values are mostly derived from galvanostatic and cyclic voltametric (CV) tests. Series resistance and frequency response are derived from electrochemical impedance spectroscopy (EIS). In this body of work, these electrode characteristics are obtained under relatively new conditions of very fast cycling through procedures designed to match the new operational envelope of the novel supercapacitors tested. Understanding the characteristics as well as the aim of the test procedures is therefore fundamental to understanding the work in this thesis.

- Capacitance (in Farads) relates to the amount of charges stored per volt of electric potential. The capacitance value from the electrode, combined with maximum cell voltage, determines the amount of energy that can be stored. Capacitance values are commonly normalized by weight (F/g) also called specific capacitance. Specific capacitance is directly related to the material and the charge storage mechanism. This value is instrumental in establishing that the electrode nano-structure is adequate for extracting all capacitive capabilities from a given material. Capacitance normalized by volume (F/cm^3) or volumetric capacitance is a measure of how compactly the active material is packed**.** Capacitance per area (F/cm^2) or areal capacitance measures the amount of charge available per unit area and it is related to material loading (g/cm^2).

Capacitance is also recorded against cycle number to determine capacitance retention, also called cycle life. High cycle life is characteristic of the extremely reversible and stress-free charge storage mechanisms found in supercapacitors. Capacitance retention can also be determined with respect to specific current (A/g). Redox-free storage mechanisms have inherently very high kinetics and can sustain higher charge/discharge currents than redox-based mechanisms. Often, carboxyl or hydroxyl groups are left on the surface of carbon electrodes; these groups store charges through a redox mechanism and contribute to capacitance concurrently with the double layer mechanism. Parasitic redox mechanisms can be selected out by varying specific current during charge and discharge. Usually the higher the current, the more stable the cycling and the longer the cycle life as only non-redox mechanisms remain active.

Capacitance mechanism performances are also scrutinized through both the shape and the mid-point discharge current of CV curves. A typical CV curve (current vs. potential) is a rectangle with sharp edges indicating low resistance. Maintaining a rectangular shape is very demanding, especially for electrode with high material loadings. CV characterizations of electrodes are routine tests and they can be conducted at high sweep rates, producing reliable sweep rate vs current graphs. In an ideal supercapacitor, sweep rate and discharge current always stay proportional. The CV test has become the procedure of choice for certifying ultrahigh-rate devices. These devices are tacitly defined as being able to maintain proportionality between sweep rate and current at over 100 V/s.

- Series impedances of electrodes with resistance lower than a tenth of an ohm produce undetectable IR-drops in galvanostatic tests with milli-amps amperages. Therefore EIS becomes the primary test to characterize series impedance. Impedance comes from both ion and electronic transport phenomena. Ionic and electronic contributions can be distinguished on Nyquist plots (Imaginary impedance vs. Real impedance). The lower the series impedance the highest the energetic efficiency. Lower impedance also allows for higher capacitance for a given RC-time constant. Low RC-time

constants are crucial to access the maximum of the charges stored in an electrode in small amounts of time.

- Frequency responses of electrodes are important for applications utilizing alternative currents like AC-line filtering. Today, these types of applications are on the verge of being accessible to newly designed electrochemical supercapacitor technologies. Frequency response is exclusively measured through EIS. EIS utilizes small amplitude (0.1 V in this work) AC-currents to probe capacitance at frequencies greater than 500 kHz through phase angle differences between voltage and current. Adequate high frequency response is defined by the ability to maintain full capacitance and low resistance characteristics at said high frequency.

1.1.2 Charge storage mechanisms

Electrochemical capacitors can store charges through three different mechanisms: in a double layer, through ion pseudo-intercalation, or via fast redox reactions. The first two mechanisms do not involve chemical reactions; ions are adsorb on or are stored inside a chemically neutral structure. The third mechanism involves fast surface reactions in metal oxide deposits or in conducting polymers in a similar fashion to Li-batteries. This is why these latter capacitors are called pseudocapacitors.

The first mechanism to be discovered was the double layer mechanism. A capacitor using it was patented in 1957 by General Electric[4]. In this mechanism electrons are forced inside a conductive material immersed in an electrolyte containing dissolved ions. Ions with opposite polarity to the electrode charges are attracted toward the electrode surface until charge neutrality is obtained. Ions tend to self-arrange in layers parallel to the electrode surface called Helmholtz layers. Charge configuration, both inside the electrode and in the electrolyte, is still very actively investigated today[14]. The first devices made utilized porous carbon electrodes and sulfuric acid as electrolyte. Since then, there have been only small improvements over the General Electric design: carbons have higher specific

surface areas and sulfuric acid can be replaced by electrolytes with a wider voltage range. Nowadays commercialised devices from companies like Maxwell, Panasonic and NessCap are indeed very similar to the first original design. With the advent of nanotechnologies, new materials have been introduced to electrochemical double layer capacitor (EDLC) applications. Novel electrodes incorporate carbon nanotubes (CNTs), graphene and other 3D-nanostructures made from other conductive sp^2-carbons[5]. Nonetheless, specific capacitance for nanomaterials stays below 300 F/g which has been readily achievable with cheaper porous carbons: CNTs manage a maximum of 80 F/g, activated graphene can reach 174 F/g and 3D hierarchical porous carbons may achieve 225 F/g[6 7]. The research efforts involving these more advanced and expensive nanomaterials have been most fruitful at enabling better charge transport and better capacitance retention at high cycle rates, expanding practical usage for supercapacitors in high power applications[43].

Cation intercalation materials suitable for supercapacitor applications have been recently discovered but they are few in numbers. One material in particular that bridges the gap between Li-battery electrodes and supercapacitors is nanocrystalline films of orthorhombic Nb_2O_5. This is a Li^+ intercalation material with two-dimensional (2-D) transport pathways that experiences very little volume changes upon Li^+ de/intercalation[8]. Also a novel family of layered materials called Mxenes was reported as pseudo-intercalation materials capable of storing a variety of ions between layers[9]. These materials are named Mxenes because of their morphological resemblance to graphene and because of their good electrical conductivity characteristics. Mxenes can store around 100 F/g but they are much denser than carbons because of their high metal content. The higher charge storage densities of Mxenes may translate in more energy dense supercapacitor devices in the future.

Pseudocapacitors were first investigated by Conway in 1975 with a study on ruthenium oxide. Pseudo-capacitance figures are far superior to EDLC's specific capacitance: for example 1300 F/g was achieved with ruthenium. Non-conducting active material is deposited on an intermediate inert current

collector, usually carbon, in very thin layers or nano-formations like nano-flowers to maximise contact with both collector and electrolyte[6]. Charge and discharge take place at the surface only a few nanometers deep in the material and they are defined as surface reactions[6]. Reactions occur in a rapidly successive manner so the overall pseudocapacitor charge storage mechanisms appear capacitive with a rectangular CV curve with no isolated peaks[6]. Several metal oxides as well as electrically conducting polymers have been tested[4, 6]. Among oxides, manganese is the most popular choice because of its low cost and the fact that it is environmentally benign[6, 7].

To conclude, it is worth noting that only EDLCs and intercalation capacitors can support thousands of cycles without capacitance fading thanks to their redox-free charge storage mechanisms. Furthermore, intercalation and most pseudocapacitor electrodes have been restricted to storing cations. Intercalation technology is theoretically capable of storing anions while most pseudo-capacitive materials cannot; expensive ruthenium oxide is an exception. In practise, both mechanisms require a counter electrode that stores anions in a traditional double layer formation. Subsequently, only symmetrical EDLCs have found commercial applications so far.

1.2 Recent improvement & approach

Electrodes for supercapacitors must satisfy three requirements: high-energy storage, low resistance and good cyclability. Successfully pursuing these qualities involves continuous investigation of fundamental phenomena (charge mechanisms, self-discharge, alkali electrolyte with potential), production of nano-structured materials (graphene, sub-nanometer pores, highly ordered CNTs) and synthesis of new materials (pseudo-intercalation Mxene, fast lithium-intercalation Nb_2O_5). This chapter reviews the published progress made that are relevant to redox-free supercapacitors and pseudo-capacitors.

1.2.1 Fundamental phenomena

Charge storage in sub-nanometer pores

A French-American research team discovered a significant increase of capacitance in sub-nanometer pores[10]. Pores of approximately the same size of ion diameter present in the electrolyte force a sieving process that strips part of the solvation layer off these ions (**Figure 1.1**). The smaller distance between ions and electrons creates an enlarged capacitance according to the following fundamental equation:

$$C = \frac{\varepsilon A}{d} \qquad \text{(equation 1.1)}$$

where ε is permittivity of the solvent, A is the total surface area, and d is the distance between opposite charges.

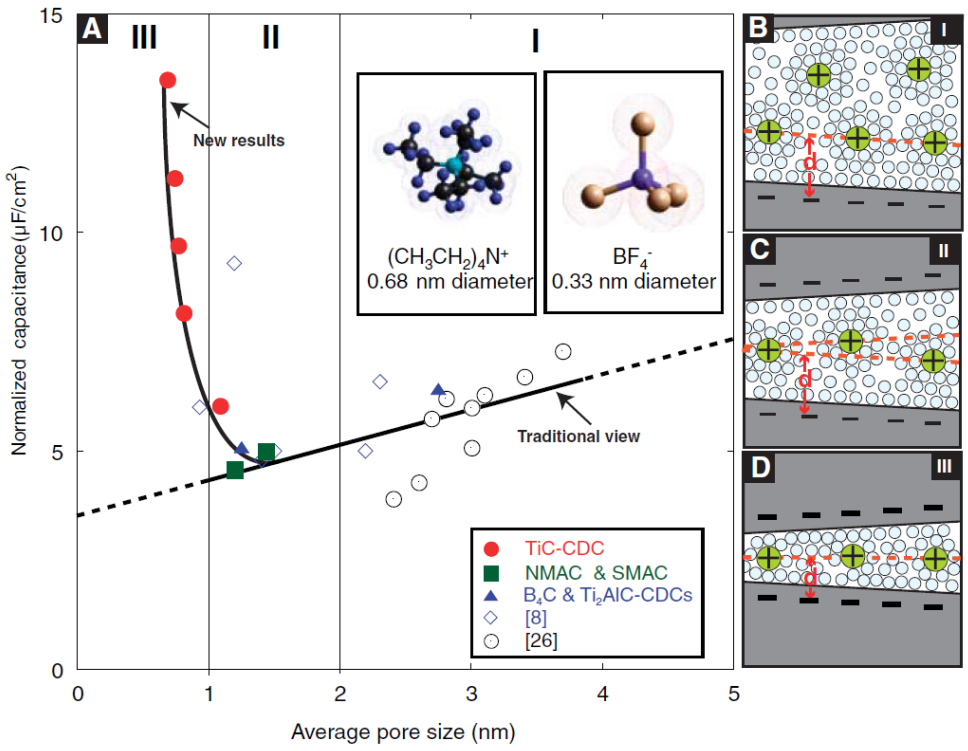

Figure 1.1 – Capacitance vs. pore size graph of sub-nanoporous carbon electrode in 1.5M tetraethylammonium tetrafluoborate in acetonitrile organic electrolyte with matching pores showing an anomalous increase of capacitance - from reference 11

Suitable nanoporous carbon can be obtained by chlorination of titanium carbide at temperature between 500 and 1000 °C. Chlorine etches out titanium ($SiC + 2Cl_2(g) = SiCl_4(g) + C$) to leave a material with a narrow pore size distribution that can be controlled with an accuracy better than 0.05-nm by varying the temperature of the chlorination process[12]. At 600 °C, the carbon pores match the effective size of the dissolved ions in the reported experiment's electrolyte[13]. Pores are shown to effectively screen ions that can enter and produce an enhanced capacitance through the partial elimination of the ion solvation layer[13]. This work has shown that pores may be tailored to increase double layer capacitance without changing the number of charges stored. No increase in the available surface area is required.

Anomalous increase of charge storage in few-layers graphene electrodes

Ruoff *et al.* conducted an experiment where double layer capacitance was created over electrodes made of only a few layers of graphene. Depending on the number of layers, the double layer capacitance varies: less graphene layers induce a rise of capacitance[14]. Similarly to sub-nanometer pores, double layer capacitance rises without the need of increasing surface area (**Figure 1.2**).

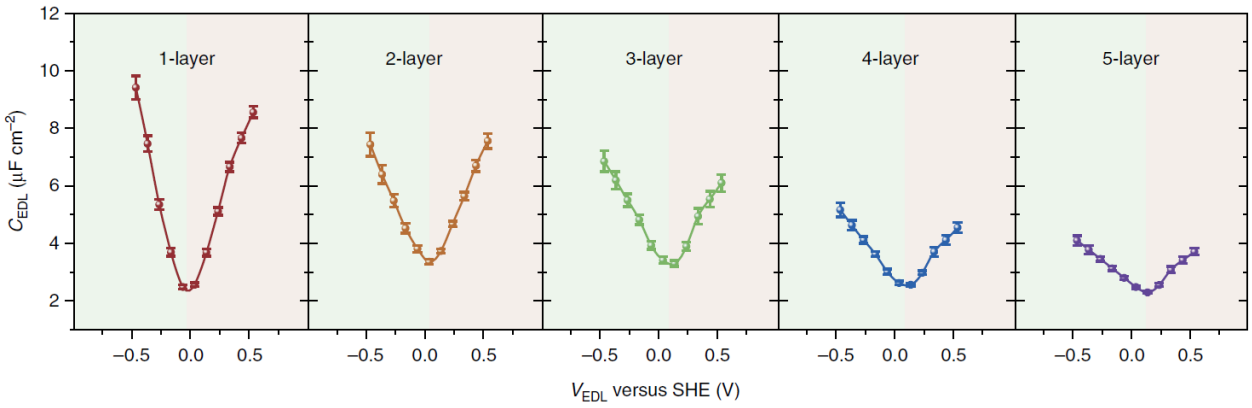

Figure 1.2 – Potential vs. capacitance graph near zero point charge of electrodes with different number of graphene layers in 6M KOH aqueous electrolyte showing much higher capacitance for electrodes with less graphene layers - from reference 14

The increase capacitance is attributed to a favorable correlation between Fermi electrons in the graphene sheets and ions in the Helmhotz layer. The resulting attractive interaction drives the thickness of the double layer down and again reduces the distance d in equation 1.1. The correlation between electrons and ions is most efficient when both types of charges are in close proximity[14]. Therefore the correlation effect is more strongly felt for thinner electrodes with less graphene layers.

For several-graphene-layer electrodes, a multi-layer charge storage mechanism develops inside the electrode[14]. These electron layers are similar to the Helmholtz layer in the electrolyte. Both capacitive

phenomena are connected in series (**Figure 1.3**). Capacitance from electron layers is calculated through charge density considerations:

$$C_q = \left| q_e \frac{\partial Q}{\partial \mu} \right| \quad \text{(equation 1.2)}$$

C_q is quantum capacitance from electron layer, q_e is the charge of an electron, Q is the total charge density, and μ is the chemical potential.

For graphene electrodes, quantum capacitance varies as chemical potential changes depending on location of each graphene layer with regards to the electrolyte interface[14]. C_q is larger for few-graphene layer electrode which in turns helps keep the overall capacitance large. Therefore it is advantageous to have very thin electrodes that prevent electron layer accumulation because accumulations draw charges further away from the electrolyte interface[14].

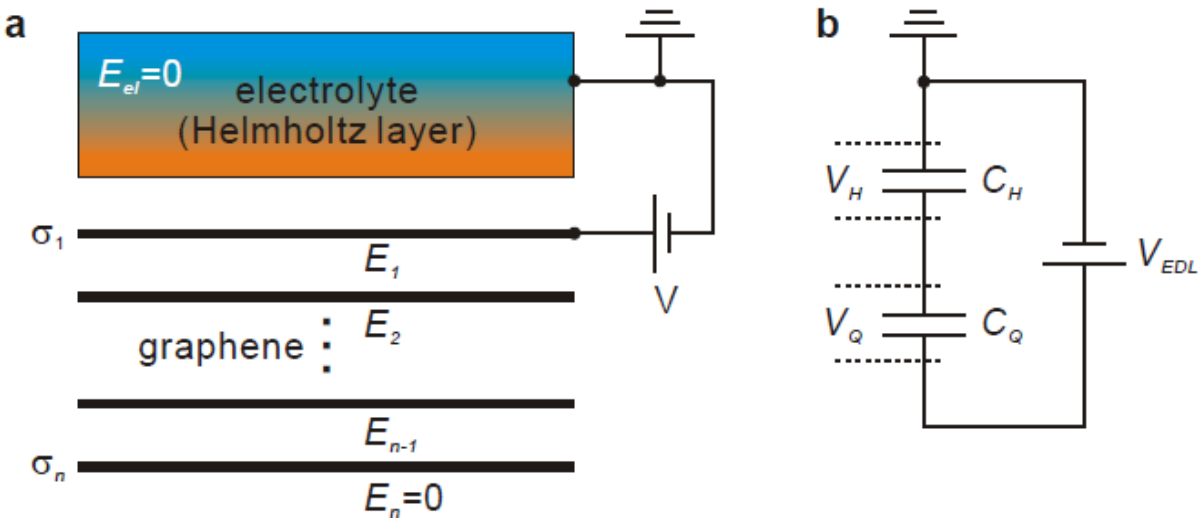

Figure 1.3 - Schematic of quantum capacitance from electrode and Helmholtz capacitance from ion double layer in series - from reference 14

Charge redistribution in porous carbon & self-discharge

Ion transport is impaired in porous and activated carbons due to the convoluted nature of the porous structure as well as the pore size distribution itself. More explicitly, ionic resistance in porous material is related to charge redistribution phenomena[15]. Small pores soaked in electrolyte in supercapacitor applications can be modeled as De Levie transmission lines (**Figure 1.4-a**).

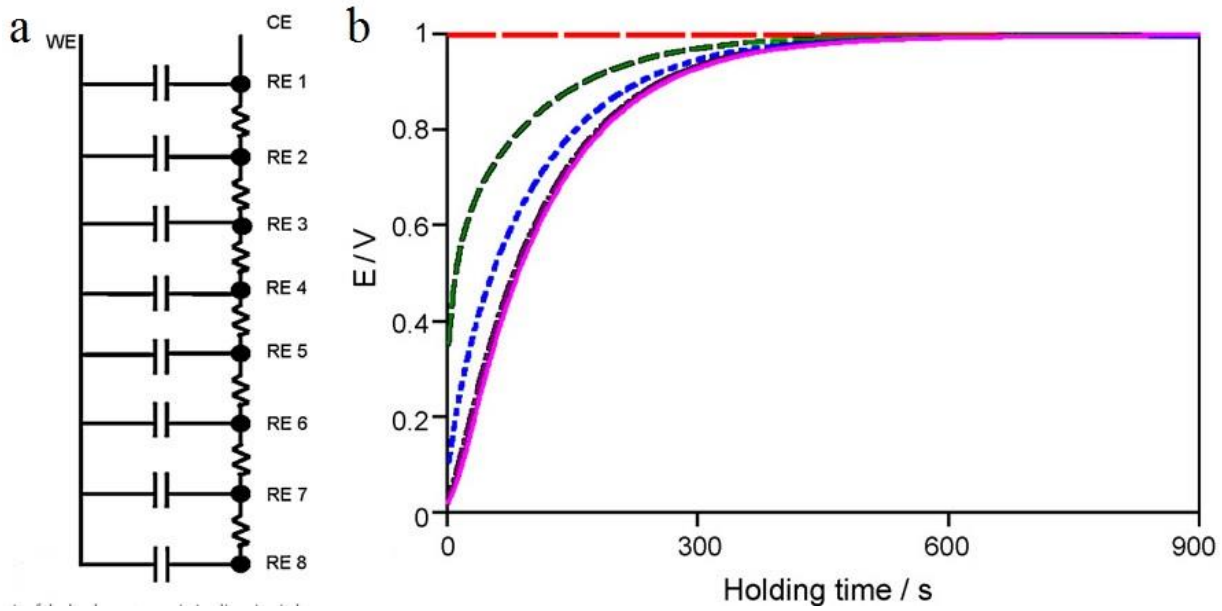

Figure 1.4 – (a) De Levie transmission line schematic representing capacitance in porous structure; capacitance: 10 µF, resistance: 50 kΩ; (b) simulated Voltage at different depths in the pores depending on holding time (red -> RE 1, green -> RE 3, blue -> RE 5, purple -> RE7, pink -> RE 8) from reference 15

The small pores of the high-surface area carbons used in supercapacitor applications cause restrictions to the movement of ions travelling down those pores. The model described in **figure 1.4** shows that ion transport is impaired by charge relocation to such an extent that full charging requires holding periods in the hundreds of seconds[15]. Holding the final voltage between the poles of the supercapacitor allow charges to propagate down the pores. The authors estimate that actual charge redistribution is about five times faster than the holding time presented in **figure 1.4-b**[15]. As a result, during charge, the mouth of the pores will store the charges first and electrode potential increase will be based on the limited but easily accessible capacitance of pore mouths. Similarly, discharge will be partial if the device is cycled quickly. Charge redistribution also affects self-discharge in supercapacitors. Superficially charged pores

will leak charges downward from the mouth to the bottom of the pores[15]. This redistribution process will lower overall electrode potential and appear like a discharge. Whereas this knowledge does not specifically pave the way toward the design of more capable electrodes, it is an explanation for the incomplete access to stored charge under cycling at high-frequencies.

Actual self-discharge in supercapacitors can be traced to iron contaminant at concentration superior to 10^{-3} Molar[16]. Dissolved iron cations shuttle between the two electrodes transforming from ferric to ferrous state repeatedly[16]. The authors were able to identify this particular mechanism by verifying that experimental discharge curves match theoretical models developed on Faradaic reactions of a diffusion-controlled species with linear discharge potential against $t^{1/2}$. Iron is a popular precursor in carbon nanotube synthesis. Therefore devices containing non-purified CNTs may suffer from self-discharge due to the residual presence of iron.

High-voltage aqueous electrolyte

Energy storage in supercapacitor is related to the square of maximum voltage:

$$E = \frac{1}{2} \times C\, V^2 \quad \text{(equation 1.3)}$$

where C is capacitance and V is potential

Aqueous electrolytes have the highest ion mobility of all other solvents, but they also have the smallest potential window. Most aqueous electrolyte applications are limited to 1.0 V because of water decomposition occurring at 1.23 V whereas organic electrolyte and ionic liquids can support voltages up to 3.5 V[17]. Recently it has been proven that aqueous electrolyte potential window can be increased by taking advantage of the strength of solvation layers: alkali solutions like 1 Molar Li_2SO_4 can operate continuously at voltages up to 2.2 V over thousands of cycles (**Figure 1.5**)[18].

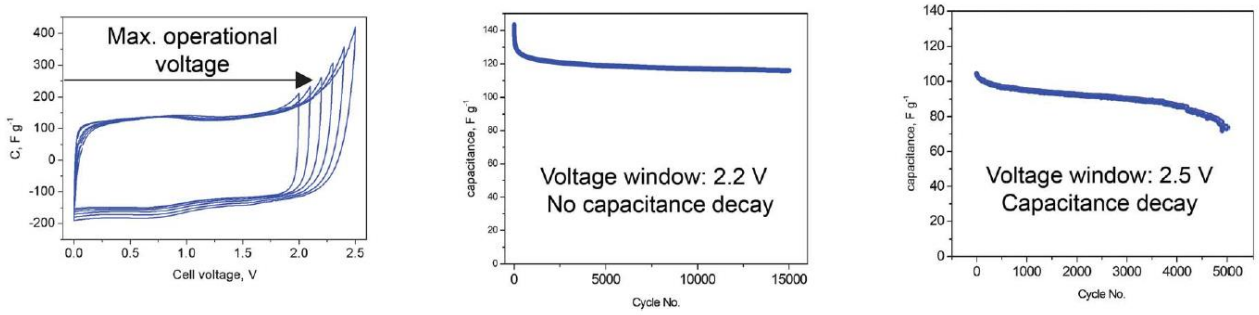

Figure 1.5 – Cyclic voltammetry tests of symmetrical carbon supercapacitor with 1M Li_2SO_4 aqueous electrolyte from 0 to 2.5 V and galvanostatic test of same system at 2.2 and 2.5 V showing cycle life - from reference 18

The increased high-voltage stability is given by the strong solvation of the lithium cation and the sulfate anion. The solvation layers have bond with energy between 160 and 220 kJ[18]. This is competitive with the energy necessary to decompose the water between 1.6 and 2.2V[18]. That strong solvation permits voltages over the theoretical potential for water decomposition in a double layer charge storage application. Extended potential windows are also reported for sodium sulfate and potassium sulfate electrolytes but to a smaller extent. The same group also achieved an increase in voltage through the use of an anti-oxidant additive, sodium molybdate[19].

1.2.2 Increasing energy storage in electrochemical capacitors

Increased surface area from graphene material

Graphene is a monoatomic sheet of sp2-hybridized carbon. As such it offers the largest specific area of all carbon materials: 2630 m^2/g. This is exactly twice the surface area of single walled carbon nanotubes (SWNTs), the next high-surface area carbon material. When charges are stored in double layers, available surface area directly conditions the amount of charges stored and therefore the capacitance. To take full benefit from the high surface area graphene was exfoliated and crumpled from graphene oxide (Figure 1.6)[20]. When 2-D materials are stacked, much of the available surface area is lost and ion diffusion pathways are restricted. Electrodes made from microwave exfoliated graphene oxide showed a surface area of 463 m^2/g; that is 6 to 9 times higher than previously reported[20]. Capacitance was measured at 191 F/g[20].

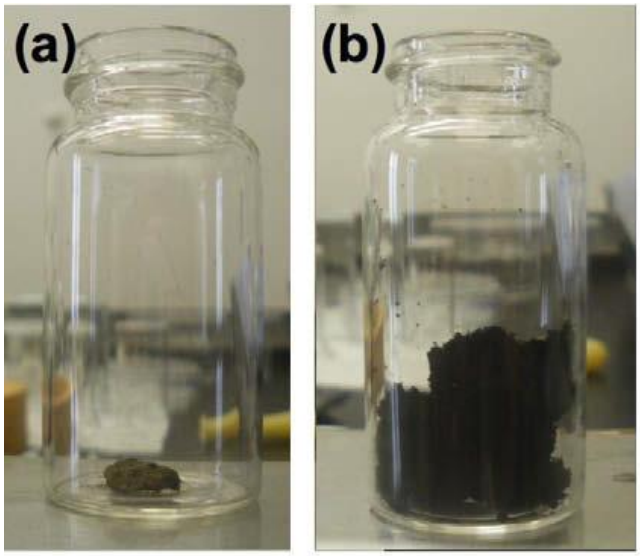

Figure 1.6 – Photographs of graphene oxide (a) before treatment – (b) after microwave treatment G.O. is reduced, exfoliated and crumpled – from reference 20

In a further development, the available surface area of exfoliated graphene was increased by KOH activation, elevating specific surface area to 3100 m^2/g[21 22]. Soon after, the group was again able to improve on their results by processing graphene oxide into hollow spheres. The final product has a specific area of 3290 m^2/g and a pore size distribution with macro and mesopores that is favorable to ion transport[23].

Electrochemical capacitor using fast redox reactions

Low capacitance of supercapacitors compared to batteries is a considerable drawback. Arguably it is the most significant reason preventing electrochemical capacitors from being adopted more widely. In that context, pseudocapacitors, that can reach 1300 F/g whereas EDLCs can only reach figures around 200 F/g, have attracted great attention from the scientific community[24]. Work is being done to realize maximum theoretical capacitance, cycle life and energy storage via higher operating voltages. Pseudocapacitance materials include metal oxides like ruthenium oxide, manganese oxide, zinc oxide, titanium oxide, cobalt oxide and also conducting polymer like polyaniline (PANI) and polypyrrole (PPy)[6]. Metal oxides are mostly non-conductive therefore they are coupled with carbon sub-structures to provide and extract electrons from the redox reactions. The conductivity impediment confines metal oxide deposits to be very small and shallow. That configuration also maximizes the exposure of reactive materials to the electrolyte allowing them to cycle relatively fast. Pseudocapacitors commonly use aqueous acidic electrolyte, mostly H_2SO_4 or alkali solutions. RuO_2 was the first oxide to be used and to be combined with activated carbons[6]. Studies by Kim and Popov showed that increasing the loading of RuO_2 is accompanied by a loss of specific area and specific capacitance because of mesopore blockage[25]. Ruthenium is also expensive and harmful to the environment contrary to manganese oxide[6]. MnO_2-CNT composites show very good capacitive behaviour[26]. Recent efforts from Yi Cui's group bear specific capacitance of 1230 F/g and 10000 cycles with 96% capacitance retention[26]. Key to this success is the

formation of extremely porous MnO_2 deposits. Composites of nickel oxide and zinc oxide with carbon nanotubes and graphene deliver similar improvements in conductivity and capacitance by acting as active sites for faradaic reactions to occur[27 28 29].

PANI and PPy conductive polymers undergo redox reactions when cycled in 2 M H_2SO_4 and deliver 240 and 530 F/g respectively. Polymers also have been combined with metal oxides as secondary current collectors, similarly to carbon sub-structures. Polymers offer the advantage of accommodating expansion and reduction of the volume of electrodes during the cycling of metal oxide particles resulting in better performance[30]. PPy-CoO composites have shown extremely high specific capacitance (2223 F/g) and relatively high cycle life (20000 cycles)[30].

1.2.3 New materials – lithium-ion and cation intercalation capacitors

The need to increase charge storage in capacitors has also driven researchers to explore the possibility of using ion intercalation materials from battery research that can bridge lithium batteries and supercapacitors with fast ion intake-release. These hybrid capacitors include a lithium intercalation material anode and a high-surface area carbon cathode. This configuration exhibits higher energy storage because of higher charge storage at low voltage combined with a larger voltage window than the equivalent symmetrical high-surface carbon device (**Figure 1.7**)[32].

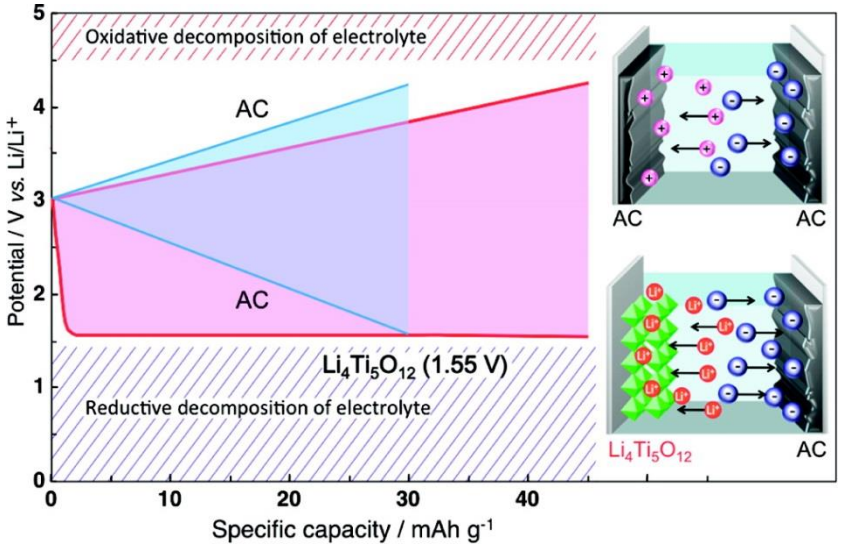

Figure 1.7 – Capacity vs potential plot comparing symmetrical activated carbon (AC) supercapacitor with hybrid LTO anode with AC cathode hybrid device both in 1M $LiBF_4$ organic electrolyte - from reference 32

The first lithium-ion capacitor utilized a $Li_4Ti_5O_{12}$ (LTO) anode and an activated carbon (AC) cathode with an organic electrolyte containing a lithium salt similar to lithium-ion battery electrolyte[31]. Conductivity quickly became an issue as internal resistance increases when LTO is delithiated[32]. $LiFePO_4$ mixed with carbon managed a capacitance of 504 F/g in 1 M $LiPF_6$[33, 34]. The addition of carbon improves conductivity and enables a charge rate of 50C (full charge in 72 seconds). Other lithium metal oxides like $LiFeSiO_2$, Li_2MnSiO_4 have been used successfully in non-aqueous lithium-ion capacitor applications[33, 34]. Similarly aqueous devices have been developed with $LiMn_2O_4$ as intercalation anode material[35]. Utilizing lithium-ion battery materials has the significant drawback of carrying over relatively low power characteristic due to relatively poor Li^+ diffusion and electrical conductivity[35]. Overcoming the conductivity problem is actively being researched as it will not only help make better capacitors but also improve lithium battery electrodes.

Previously introduced in sub-chapter 1.1.2, Nb_2O_5 nanocrystal films is the lithium intercalation material most capable of serving as capacitor electrode with charge rate reported at 1000 C (full charge in 3.6 seconds) in 1 M $LiClO_4$ organic electrolyte[8]. This extraordinary rate is obtained through a facile insertion of Li^+ cation through (001) polyhedral planes of the crystal structure (**Figure 1.8**)[8]. The capacitance obtained through intercalation is similar to that offered by LTO hybrid capacitor: 40 mAh/g. But the intercalation mechanism behaves closer to metal oxide pseudocapacitors with surface reactions like RuO_2.

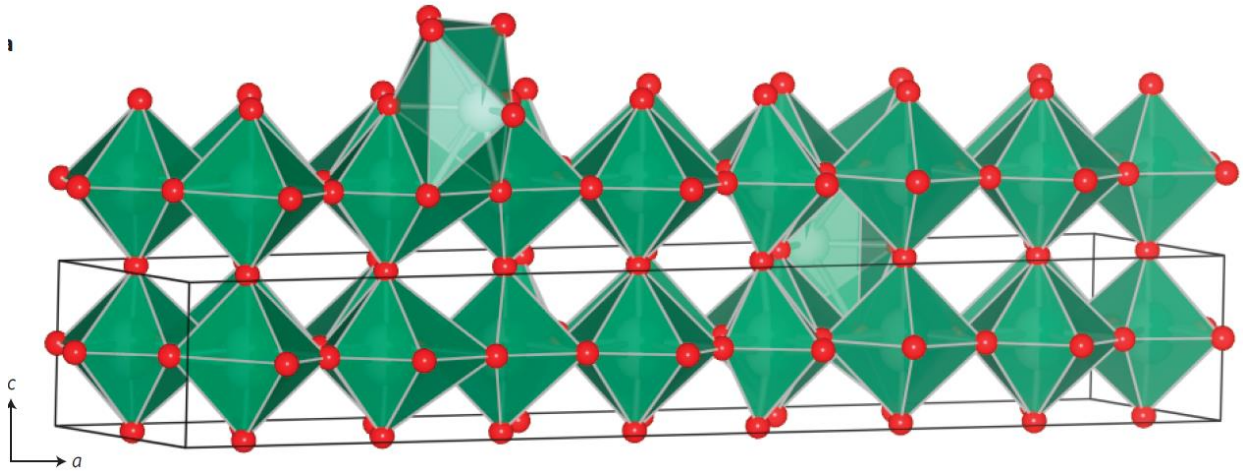

Figure 1.8 – Representation of crystal structure of Nb_2O_5 with oxygen in red and niobium contained inside green polyhedral. Lithium cations can move easily in the space in the a-b plane – from reference 8

Mxene materials obtained from extracting a III A or a IV A element from layered carbide MAX phases are novel materials that can also serve in capacitor applications[9]. Mxenes are 2D materials capable of storing cations between layers of materials in a pseudo-intercalation manner (**Figure 1.9**)[9].

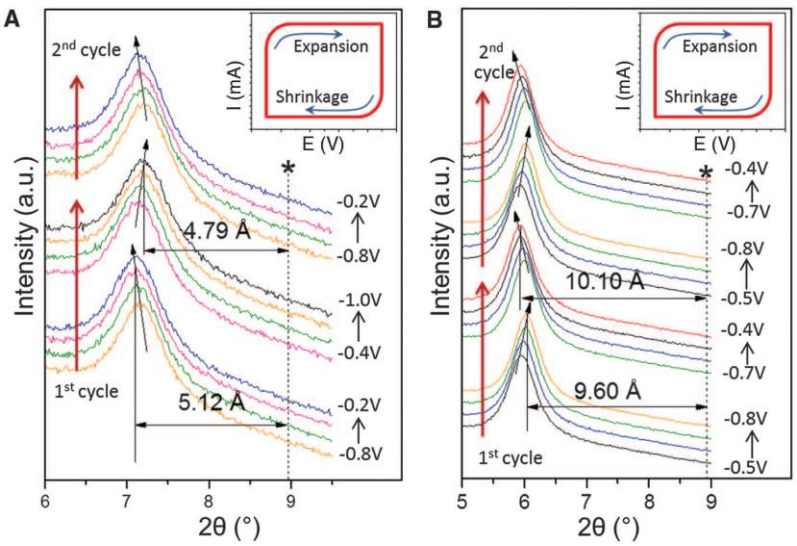

Figure 1.9 – In-situ X-ray diffraction of Mxene $Ti_3C_2T_x$ cycled in: (a) 1 M KOH aqueous solution, (b) 1 M $MgSO_4$ aqueous solution. Stared line represents the relative position of layers before immersion – from reference 9

Mxene pseudo-intercalation capacitors can have up to 140 F/g pf specific capacitance with no detectable loss over 10000 cycles. These capacitors are asymmetrical with a high-surface area carbon counter-electrode[9]. Pseudo-intercalation is less sensitive to the size of cations and Mxene have been shown to be able to store a large variety of cations[9].

1.2.4 Effective charge transport advances

In the early 2000s, as advanced materials with nearly optimal specific surface area like graphene and single layer carbon nanotubes were used, increasing performance of double layer electrochemical capacitors further relied on improving charge transport in and around electrodes through advanced nanostructuring[41]. Charge transport phenomena include ionic movements in the vicinity of electrode surfaces, electronic conductivity in the bulk as well as electron collection through interfaces[43].

Aligned carbon nanotube structures

It has been widely recognized that incorporating insulating binders in electrodes that also block ion passageways was limiting both specific capacitance and frequency response capabilities (**Figure 1.10**)[36 37 38]. Aligned CNTs, also called CNT forest, is a sophisticated carbon arrangement that has been actively pursued for making electrodes since the late 2000s. Aligned forests of CNTs were selected as a way to optimize available surface area as well as facilitating ion movement around the CNTs[39]. Because of the regular structure, ion transport is facilitated. Electrodes made from aligned CNTs have lower series resistance and support higher sweep rates than equivalent entangled CNT networks[40]. A more recent study on CNT forest electrodes also determined that equivalent series resistance (ESR) is reduced and the specific capacitance is increased when the length of tube is shortened[41]. It was also reported that ESR is also reduced effectively through vertical compression of the forest[41]. The deformation changes the morphology at the base of the tubes increasing contact area with the current collector. Combining both short length and compressed tube base decreased ESR by 67%[41]. Furthermore, depositing a thin layer of platinum at the base of the tubes, close to the contact with the current collector, decreased ESR by another 9%[41].

Recently a group from Texas produced a carpet of carbon nanotubes grown on a graphene sheet with excellent results: nearly ideal capacitance behaviour up to 120 Hz and constant capacitance maintained up to 100 V/s sweep rate[42].

Aligned carbon nanotube structures are an efficient way to improve charge transport. They also augment our knowledge about making better contacts with current collectors. But making CNT forests is unfortunately expensive and non-scalable.

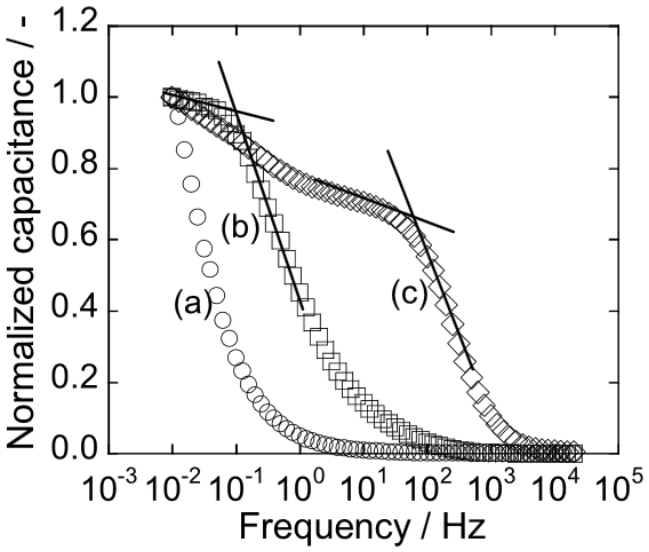

Figure 1.10 – EIS tests showing capacitance frequency response of electrodes in triethylmethylammonium tetrafluoroborate in propylene carbonate organic electrolyte made from: (a) activated carbon, (b) disordered multi-walled carbon nanotubes, (c) vertically aligned multi-walled carbon nanotube – from reference 38

Vertically aligned graphene sheet

Graphene can also be oriented vertically to enhance ion transport. This architecture increases supercapacitor performance dramatically to the point where a macro-device can cycle at 120 Hz enabling the filtering of AC power lines[43]. Before this architecture was developed, AC-line filtering and other high-frequency applications like the starting of AC electric motors have been handled by electrolytic or other types of capacitors with lower energy storage abilities. Vertical graphene sheets can either be grown through a high-temperature chemical vapour deposition (CVD) process or deposited from a graphene oxide suspension reduced electrochemically reduction and directly on a gold current collector from an aqueous solution[43 44 45]. Vertically oriented graphene electrodes are the most capable double layer charge storage architecture in terms of frequency response and operation at very high sweep rates. These electrodes show electronic impedance too small to appear on Nyquist impedance

plots: no semi-circle (**Figure 1.11**). The production of graphene via high-temperature CVD is accompanied by diffusion of carbon atoms in the current collector[44]. Electrodes made using this technique are capable of frequency response reaching over 20 kHz at -45° [44]. However ultimate capacitance from any graphene electrode is limited because of obstruction of ion paths arising from stacking many graphene sheets[45].

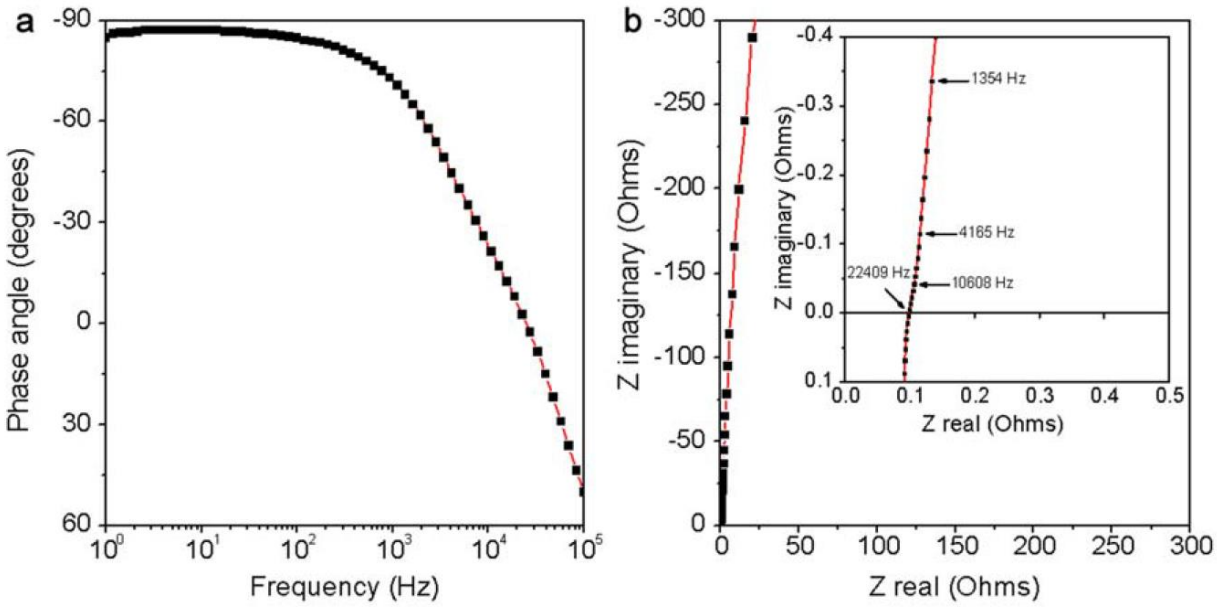

Figure 1.11 – EIS tests of vertically aligned reduced graphene sheets in 25% KOH aqueous electrolyte: (a) phase angle vs. frequency plot; (b) Nyquist complex plane impedance plot – from reference 45

1.3 Summary

Since supercapacitors were first invented when capacitors electrodes were paired with a battery electrolyte in 1957, innovations in the field have successfully employed many other materials developed originally for battery applications[4, 6]. Also, continuous research efforts have move our understanding of

EDLC charge storage from a strict double layer described by Helmholtz in 1853 to the Stern diffuse model in 1924 and finally to a model that encompasses contributions from ion solvation layer and quantum capacitance still being developed today[14]. Novel charge storage mechanisms have been introduced: lithium intercalation, cation pseudo-intercalation and fast surface redox reactions[6]. These later innovations were again inspired and derived from past battery developments which have been adapted to capacitor applications. Battery-derived mechanisms have brought vast improvements in terms of amount of charges stored and extension of working potential[32]. Capacitors have gained much higher energy storage from li-battery technologies. However, battery technologies inherently carry over lower charge transfer capabilities that must be remedied so that they may become fully compatible with the expected qualities of capacitors: high charge flow, fast charge and discharge capabilities and long cycle life. Present day pseudocapacitor electrodes have limited active material loadings and lithium-ion capacitors routinely display cycle life two orders of magnitude lower than that of the best double layer capacitors[26]. Most of the current problems reside at the micro-and nano-level where charge transfers, whether ionic or electronic are not optimized and are still relatively restricted and can be optimized further. Some breakthroughs have been had, like nano-size deposition of metal oxide particles on carbon, and using polymers that can accommodate volume changes during cycling thus retaining good contact throughout[6, 30]. In conclusion, a continuing effort on improving charge storage and extending energy storage is still important, but ensuring adequate, fast and efficient charge transfer is taking more and more precedence in capacitor research and development.

1.4 Scope of research presented in this thesis

This thesis presents an original body of work that focuses on charge transport enhancements; particularly on the causes and the effects of improvements gained in conductivity through an innovative

method for making highly-conductive CNT-composite electrodes. ***Chapter 1*** has introduced supercapacitors as well as the most important recent approaches and technologies researched. ***Chapter 2*** describes the electrochemical techniques and material characterisation methods employed in the work presented here. ***Chapter 3*** presents the first CNT-based electrodes capable of AC-line filtration. These electrodes were made using an innovative dispersion of pristine CNTs combined with surface treated current collectors. ***Chapter 4*** examines novel composite electrodes using CNTs as highly conductive binder to Ti_2C Mxene pseudo-intercalation material for capacitor application. Finally, the contact impedance of the 2-D Mxene material to metal current collector is compared to that of 1-D pure CNTs to the same current collector.

CHAPTER 2 – CHARACTERIZATION METHODS AND TECHNIQUES

2.1 Electrochemical techniques

2.1.1 Electrochemical cell configuration

Two electrode configurations were used in this work: two- and three-electrode types. Both types were made with Swagelok™ holding parts and casings. Current collectors were 1.2 cm-diameter metal rods with and without gold coating.

Three-electrode cells add a reference electrode: a Sigma-Aldrich silver-silver chloride electrode with 3-molar potassium chloride (cf. **figure 2.1**). Active materials are conditioned without polymer binders, either in self-standing films or grounded in powders directly deposited on a glass fibre separator. Active materials are prepared in air at room temperature. Self-standing films are affixed to metal rods under a standard pressure of 22 MPa using a Carver™ press. Electrolytes are prepared with diluted hydrochloric acid or alkali salts dissolved in Milli-Q™ water with 18 MΩ resistance.

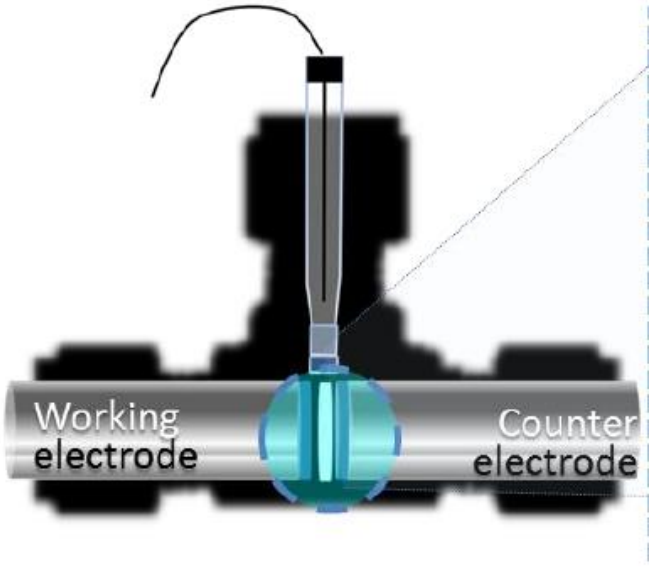

Figure 2.1 - Configuration of three-electrode cell used in the work reported in this thesis – from reference 46

2.1.2 Galvanostatic cycling

In this electrochemical test, charge and discharge currents are imposed and the voltage is recorded. Voltage will increase during charge under a constant current until it reaches a preset threshold. Then the current will be reversed to discharge the cell. The voltage will decrease until it reaches a second pre-set threshold and the cycle will be repeated. The number of cycles is decided in advance by the operator. Charge and discharge currents can be set independently although they have always the same absolute value in this work. Capacitance is obtained with very good accuracy from galvanostatic cycling because currents can be set precisely from a few μAs to hundreds of mAs. Capacitive mechanisms with no redox charge have constant capacitance at all potential values therefore the voltage vs time curve is an exponential with no intermediate plateau. Galvanostatic testing is one of the most used cycling methods for determining capacitance and cycle life in supercapacitors because

capacitance can be tracked from cycle to cycle. Cycle life plots are graphs of capacitance calculated at each given cycle vs cycle number. For non-reactive charge storage mechanisms, this graph should present a constant horizontal line over cycle numbers approaching one million. This characteristic confirms that the capacitance seen is from a redox-free mechanism. For more complex and less robust mechanisms, capacitance may drop sooner. Galvanostatic cycling allows probing performance of devices under increasing values of specific current. Capacitance retention under high specific currents tests the suitability of electrode designs when the active storage mechanisms are fast like double layer charge storage mechanism (this study is presented in chapter 3). Galvanostatic tests enables probing a new mechanism for high current capability (that study is presented in chapter 4). Galvanostatic cycling is done on a Biologic™ VMP3 or MPG potentiostats and analysed through EC-lab™ software.

2.1.3 Cyclic voltammetry

Cyclic voltammetry is an electrochemical test designed to apply a voltage ramp between the poles of a cell and record induced currents. In practise, a voltage ramp is set between two predefined potential limits. Potential is swept from the lower limit to the higher limit and then immediately reversed back to the lower limit. Arbitrary number of cycles can be specified. Cyclic voltammetry tests, or CV tests, can be conducted on two- or three-electrode cells. In this thesis, both types of cells are tested. The original intent of this test has been to characterize the potential at which redox reactions occur in cells. Therefore potentiostats are very accurate at relatively small voltage ramps (<100 mV/s) also called sweep rates. At the other end, electrochemical capacitors do not produce the current peaks characteristic of redox reactions. For capacitors, electronic current value at the mid-potential point is the only relevant quantity and testing their fast charge/discharge qualities requires large sweep rates. Cycling at fast sweep rates (>1 V/s) is essential to characterize the ability of supercapacitor electrodes to maintain constant capacitance under high operating currents. CV tests provide comprehensive

information on capacitance performance of charge storage mechanisms throughout the entire potential range offered by the electrolyte. And CV measurements are also the most reliable technique to determine the maximum specific current tolerable by novel electrode architecture, material and charge storage mechanism systems.

Ideal capacitors shall maintain both, identical constant charge and discharge currents, as well as unbroken proportionality between current and sweep rate. It follows that a CV curve for a supercapacitor must have a rectangular shape. Supercapacitors with low series resistance experience very large currents when cycled in CV tests. Therefore controlling the amount of active material tested in this work was critical not to exceed equipment limitations. The same equipment and software used for galvanostatic test is used to perform and analyze CV cycling. Limits for the Biologic VMP3 potentiostat are 200 V/s for quantitative results (e.g. discharge current metrics), and greater than 1 kV/s for qualitative characterization (e.g. CV curve overall shape).

2.1.4 Electrochemical impedance spectroscopy

Electrochemical impedance spectroscopy, or EIS, is an electrochemical procedure that measures the complex impedance of dipoles. Complex impedance of a device is related to its resistance, capacitance and inductance. In EIS analysis, an alternating signal is applied to an electrochemical cell and the response is recorded. Being an AC process, EIS can only be applied to two-electrode cells. In this work a sinusoidal voltage excitation is applied over a range of frequencies with constant amplitude of a few millivolts. A bias direct current (DC) voltage can be specified so that electrodes can be analyzed at different voltage points over their potential range. When probed by small voltage amplitude, all impedance processes appear as linear. Therefore EIS is better representative of interface electronic resistance and ion transport in electrolyte when used in supercapacitor applications. Because of the small amplitude, charge storage mechanisms are probed under quasi-static charge movements. These

small excitations are only representative of full-charge cycling for processes defined as being completely linear like the double layer mechanism for example.

The results from EIS analysis are routinely presented as Nyquist plots with Imaginary vs. Real parts of impedance. For a supercapacitor, the characteristic curve is formed of a semicircle at high frequencies followed by a nearly vertical line at low frequencies. The ends of the semi-circle intersect with the real axis and represent series resistances of the device. The left-most point is related to ionic contribution only, and the width of the semicircle corresponds to electronic contribution to total series resistance. The height (Imaginary impedance) of the nearly-vertical line is related to ultimate capacitance.

EIS results can also be presented as a graph of capacitance vs. frequency or phase angle vs. frequency. When an ideal capacitor is excited with AC voltage, it will respond with AC current that is -90° out of phase with voltage. An ideal resistor has AC voltage perfectly in phase with current (i.e. 0° phase angle). Therefore phase angle vs. frequency graph is instrumental into specifying how a device behaves at critical frequencies such as 120 Hz in AC-line frequency applications. In this thesis, cells are tested with frequency ranging from 500 kHz to 100 mHz, amplitude of 5 mV with 0.1 V DC bias for cells in Chapter 3 and no bias in Chapter 4. EIS measurements were carried out on Biologic™ VMP3 stations and data were analysed with EC-lab™ software.

2.2 Material characterization

2.2.1 Thermal gravimetric analysis

Thermal gravimetric analysis (TGA) is performed by heating samples to very high temperatures (up to 1200 °C) and recording weight loss as well as heat absorption. TGA can accurately characterize phase transition points of materials using cantilever balances sensitive to microgram changes in weight. TGA employs a comparative two-pan system where weight loss of a sample placed in one pan is determine versus the weight of a reference empty pan placed in the same temperature and atmosphere conditions. TGA can also identify the percentage weight content of a particular compound in a sample thanks to the known evaporation temperature of said compound. In energy storage research, performance is routinely normalized per weight of active material. This is the basis for comparison with other technologies, therefore accurate weight measurements are paramount. In this thesis, TGA was utilized to accurately determine the weight content of active materials in composite films. Films were heated in air from room temperature to 800 °C with a standard 10 °C/min linear temperature ramp. Carbon content was determined through weight loss between 200 and 400 °C. The equipment used was a TA instrument™ SDT Q600 analyzer placed on a heavy table with granite top.

2.2.2 Scanning electron microscopy

Scanning electron microscopy (SEM) uses a focused electron beam to image conductive samples through secondary and backscattered electron emissions coming off the material. SEM machines usually use a heated tungsten filament as primary source for electrons. These electrons are accelerated in a strong electric field where they gain energies up to 40 keV. The accelerated electrons are directed by electromagnetic lenses (condenser) to form a focused beam. That beam is then raster scanned across the sample in the same way images are formed on the screen of a cathode-ray tube monitor. The

electrons hitting the sample excite its atoms that in turn emit secondary electrons. Re-emitted electrons are detected with a photomultiplier using a scintillator to convert electron impacts into light. The size of the interaction volume can exceed 100s of nanometer and it depends on the energy of the electron beam. Each scan point will produce a different intensity that will result in a monochromatic image of the sample. SEM can resolve details down to about 1 nm.

Electrons from the beam must pass through the sample and be evacuated into the metallic mounting plate to prevent electrostatic build-ups. Therefore samples have to be conductive otherwise images would very quickly turn white from saturation. In this thesis, we image exclusively very conductive electrode materials. The single walled carbon nanotubes we use in our electrodes are just over 1 nm in diameter. The small size prompted us to use lower beam settings to get better resolution at the expense of contrast. We use a Zeiss LEO 1530 and a Zeiss Ultra Plus machine to image composite electrode material. SEM images give information about particle and apparent pore sizes on the surface of the material. Another critical information given by SEM is film thickness which is used to calculate energy and capacitance volumetric densities.

2.2.3 Raman spectroscopy

Raman spectroscopy is a technique that uses an infrared laser to probe molecular vibrational modes in a sample. These vibration modes relate directly to the types of covalent bonds present in the analyzed material. The photons from the probing laser scatter with the sample's molecules and impart changes to molecule vibrational modes. Scattered photons will come out with either a higher or a lower wavelength depending on if the struck molecule recovers into a more or a less energetic vibrational state than before the scattering event. The results are generally presented in the form of a graph with intensity vs. energy shift, with shifts expressed in inverse centimeters. Raman spectra of materials like CNTs are very well known. Peaks at specific energies have been matched to structural defects and the

presence of functional groups on the surface or the ends of the tubes (i.e. bonds with other atoms like oxygen). Raman spectroscopy is used in this thesis to confirm that carbon nanotubes have not been altered after they have been dispersed in chlorosulfonic acid. The equipment used is a LabRam™ HR system (Horiba Jobin Yvon) equipped with an upright microscope and a piezo sample stage and a 632.8-nm wavelength laser.

2.2.4 Fourier transform infrared spectroscopy

Fourier transform infrared spectroscopy or FTIR is conducted using infrared laser light similar to Raman spectroscopy. For that reason, FTIR spectroscopy probes similar molecular and atomic bond qualities as Raman and both tests are complementary. In FTIR spectroscopy, signal is not monochromatic and contains many wavelengths. Light intensity transmitted through the sample is passed through a Michelson interferometer to differentiate between all frequencies. Molecular vibrations are responsible for absorption of light at different wavelengths. The results first obtained in temporal domain are transferred to frequency domain via Fourier transform. FTIR graphs are similar to Raman graphs: they present signal intensity versus wavelength in inverse centimeter. In this thesis, we conduct a comparative FTIR study to further prove that CNTs have not suffered chemical functionalization after exposure to acid dispersant. The equipment used was Bruker Tensor™ 37 under air atmosphere.

2.2.5 X-ray diffraction

X-ray diffraction or XRD is a very popular technique in material science. It is a non-invasive structural characterization of materials. XRD works by reflecting an X-ray beam off the crystalline planes of a sample. Outgoing X-rays interfere constructively or destructively. The final signal is recorded. Interferences change depending on the relative angle between rays and crystalline samples because the

distance travelled by X-rays scattering off planes with fixed spacing varies with the relative angle. The probing X-rays have a known wavelength. Interference patterns are described by Bragg's law:

$$n\lambda = 2d \times \sin\theta => d = \frac{n\lambda}{2\times\sin\theta} \quad \text{equation 2.1}$$

θ is the angle between incident X-rays and parallel crystal planes, d represents the distance between crystalline planes and λ is the X-ray beam wavelength.

In operation, incidence angle is swept continuously and X-ray intensity peaks are recorded. These peaks correspond to constructive interference at given angles. From the angular position of the peaks, planar distances in the sample are derived and the sample can be identified. It worth noting that samples are mostly powders with crystals in random directions. Despite the random orientations, the diffraction process does work well with powders and the pattern given by the instrument is representative of the material because inter-planar distances remain consistent.

Inter-planar distance is a defining characteristic of inter-planar bonds in 2D materials like Mxene phases. In this work, XRD is used to partially specify that 2D Ti_2C is unaffected by dispersion in acid. XRD patterned were collected on a Bruker™ D8-Advance diffractometer with Cu-Kα radiation ($\lambda = 0.15405$ nm) and powder samples were placed on a "zero-background" holder.

2.2.6 Brunauer-Emmet-Teller surface area characterization

Brunauer-Emmet-Teller surface characterization or BET is a surface analysis technique that relies on nitrogen gas adsorption to determine surface area. The pore volume and pore size distribution of a given material can also be determined through gas adsorption measurements using density functional theory. Nitrogen adsorption and desorption isotherms are collected at liquid nitrogen evaporation temperature (77 K) over a range of relative low pressures. Nitrogen is injected in an evacuated quartz tube containing a sample of known weight. Nitrogen will adsorb on the entire surface of the sample. The amount of molecular adsorption recorded depends directly on the surface area available. Isotherm

collection is a comparative process where gas adsorption in the tube containing the sample is compared to an identical but empty reference tube. Prior to obtaining a measurement, sample must be degassed and dried thoroughly. In this thesis, carbon and Mxene samples are dried and degassed at a minimum of 120 °C during 30 minutes under vacuum.

Accurate specific surface area and pore size distribution measurements are at the heart of charge storage mechanisms in supercapacitors, especially the double layer mechanism. Measurements were conducted on a Quantachrome™ Autosorb-1 with multi-point analysis.

2.2.7 X-ray photoelectron spectroscopy

X-ray photoelectron spectroscopy or XPS is a very powerful tool for characterizing atomic bonds and environment. The process is based on the photoelectric effect: electrons escape materials when they are excited by high energy photons. The exciting beam is X-ray. Upon being hit by photons, atoms are taken away from ground energy state and emit core electrons. XPS measurements require a very high vacuum to limit the loss of emitted electrons to collisions with gas molecules. Escaping electrons are then measured for kinetic energy. That value gives information on the target binding energy. Energy transfer is described by the following equation:

$$E_{binding} = h\nu - E_{kinetic} - \Phi \quad \text{equation 2.2}$$

$E_{binding}$ represents the binding energy of an emitted electrons in its ground state, $h\nu$ is the photon energy from the X-ray beam, $E_{kinetic}$ is the measured kinetic energy of the emitted electron, and Φ is the work function from the spectrometer used in the energy detector.

A detector records the kinetic energy of emitted electrons coming towards it. Because emissions are random, intensity in one arbitrary direction is directly proportional to the entire number of emissions. Every atomic bond produces a different energy peak in XPS which also depends on the environment of the atom. Accurate reference charts of various atoms in different chemical

environments are maintained by the scientific community. These XPS charts are matched with new experimental results and information on the chemical environment of a particular atom is determined. Chemical compositions as well as covalent bonds between different atoms can be identified.

X-rays only interacts 10-nm deep inside the sample, making XPS effectively a surface characterization technique. In this thesis, XPS is used to probe oxidation state of current collectors with different surface treatments. All measurements were conducted on a Thermo VG Scientific ESCALab™ 250 XPS microprobe system with a monochromatic Al Kα (1486.6 eV) 150 W X-ray source with 0.5 mm circular spot size.

2.2.8 Atomic force microscopy

Atomic force microscopy or AFM is an imaging technique based on proximity forces. A sharp tip is positioned against or near the targeted sample surface and then scanned across. The nano-sized AFM tip is mounted on a cantilever that deflects when the tip is traveling on or near a surface topographic feature. The forces acting on the tip can come from direct contact or from proximity forces like Van Der Waals, electrostatic or magnetic forces. The position of the cantilever is monitored by a laser reflecting off its back and onto a sensor. The combination of the nanometer sized tip and accurate laser positioning endow AFM with sub-nanometer resolution capabilities. AFM is an invaluable tool for surface nanotopography. Unlike SEM imaging, AFM is able to measure the dimensions of peaks and troughs accurately. On the other hand, the total area that can be scanned is on the order of a few micrometer squares which is much less than what can be done with SEM. Also the acquisition time with AFM is much longer.

In this thesis, AFM is used to examine 1 μm^2 patches of the surface of metal current collectors at the nano-level. The metal samples have different surface treatment and roughness. Images are obtained

from averages over 512 passes. A MultiMode™ Scanning Probe Microscope with Nanoscope™ controller from Digital Instrument Veeco™ Metrology Group was used in this thesis.

2.2.9 Contact profilometer

Contact profilometers are instruments built for the unique purpose of recording surface roughness mainly at the micro-level. Profilometer operations are usually contact-based and they use a sharp nano-sized tip similar to the tip found in AFM instruments. Profile measurements can also be made with non-contact optical techniques. Profilometers are used to scan samples across distances up to 50 mm with vertical range of a few hundred micrometers. This is to be compared to the total travel of hundreds of nanometers of vertical range of typical AFM measurements.

In this thesis a contact profilometer was used to scrutinize surface roughness of metal current collectors at the micro-level. A Dektak™ Stylus 8 was used. Full travel of the contact element was restricted to a maximum range of 6.5 μm and 4.4 mg of weight was applied to keep contact with the sample.

CHAPTER 3 – COMPOSITE CARBON FILMS WITH CARBON NANOTUBE BINDER AS A HIGH-PERFORMANCE ELECTRICAL DOUBLE LAYER SUBSTRATE FOR SUPERCAPACITORS

3.1 Introduction

As mentioned in chapter 1, double layer formation remains limited by phenomena obstructing charge transport and preventing this form of charge storage from reaching its full potential. Therefore one significant aspect of supercapacitor research has been about reducing series resistance. Numerous attempts have been carried out using novel carbon materials and electrode architectures. In particular, carbon nanotubes (CNTs) which exhibit excellent electronic conductivity and fast ionic transport that are optimized by the natural occurrence of mesoporous mesh-like frameworks when they are stacked. These frameworks can retain full charge storage capacity at higher frequencies than porous carbons (PCs) or graphene alone[47, 48, 49]. PCs have very high surface area but relatively low conductivity both electronic and ionic owing to their convoluted pore structures. As for graphene-based supercapacitors, despite a high gravimetric energy density, low volumetric energy density limits their capacitance per unit area. This is due to the fact that stacking sheets quickly limits ionic transport[45]. Composite films of different carbons have also been pursued in an effort to combine complementary strengths. For example, CNTs and graphene composite have been shown to demonstrate good ionic conductivity and high volumetric energy density, and the addition of CNTs to PCs was reported to yield improved electronic conductivity [21, 7, 22].

Recently, new developments in supercapacitor technology have led devices functioning on the double layer charge storage mechanism to fulfill the stringent frequency response requirements of AC-line filtering applications[43]. These requirements revolve around maintaining full capacitance behaviour at 120 Hz that is possible with very low internal resistance. The devices published so far are very capable and, despite the inherent energy density limitation, are all based on graphene[43, 44]. Furthermore no explanations have been offered about how the very low overall series resistance, critical to the devices' newly found performance, is obtained. The graphene limitation in energy density, as well as the lack of understanding about the charge transport improvement achieved triggered the development of AC-line filtering capable composite CNT-based electrodes with a nanostructure constructed via a discrete process. A step-by-step construction of electrodes enables us to provide insight about charge transport through each component of the carbon electrodes and discover critical charge transfer bottlenecks.

A highly conductive electrode design was created by producing a dispersion that preserves the electrical conductivity of single-walled CNTs while delivering the required mesoporous network film through filtration, and by attaching these films on specially tailored current collectors. Aside from imparting good ionic conductivity, single-walled CNTs are simultaneously used as a highly conductive binder for other sp^2-carbons. Non-permanently functionalizing chlorosulfonic-acid dispersion and filtration techniques reported respectively by Pasquali *et al.* and Hetch *et al*[50, 51]*.* for graphene and CNTs are employed and applied to mixtures of different sp^2-carbons. The resulting mesoporous carbon films are free from the inherent areal capacitance limitations experienced by graphene-based devices. Films are then pressed onto polished, roughened, and gold coated stainless steel current collectors to study the effect of specific collector surface treatments. This chapter exposes the crucial role of creating extensive contact points between metal current collectors and the dry, binder-free, self-standing active materials increasingly used in high-power supercapacitor and battery applications. Ultimate charge

transfer abilities are proven to be highly dependent on surface chemistry and roughness of the metal at the current collector/carbon interface.

Discussions and guidance from Professor Shirley Tang about carbon nanotubes properties and fourier transform infrared (FTIR) characterisation are acknowledged.

3.2 Experimental

3.2.1 Binder-free carbon films, electrode and cell preparation

Single and hybrid carbon films were made by combining the methods of Pasquali et al on dispersion and of Hetch *et al.* on filtration[50, 51, 52, 53]. CNTs and Ketjen black PC were dispersed in 99% chlorosulfonic acid (CSA, Sigma-Aldrich) and stirred overnight, then the colloidal dispersions were vacuum-filtered through alumina filters (Whatman™) with pores of different diameters: 0.02 µm for single walled carbon nanotube (SWNT) films (**Figure 3.1-a**), 0.1 µm for SWNT-MWNT (single and multi walled carbon nanotube composite or S-MWNT) films (**Figure 3.1-b**), and 0.2 µm for SWNT-AC films (**Figure 3.1-c**). Films were rinsed with chloroform (> 99.8%, Sigma-Aldrich) before using a DI-water bath to float the hydrophobic films and separate them from the filters.

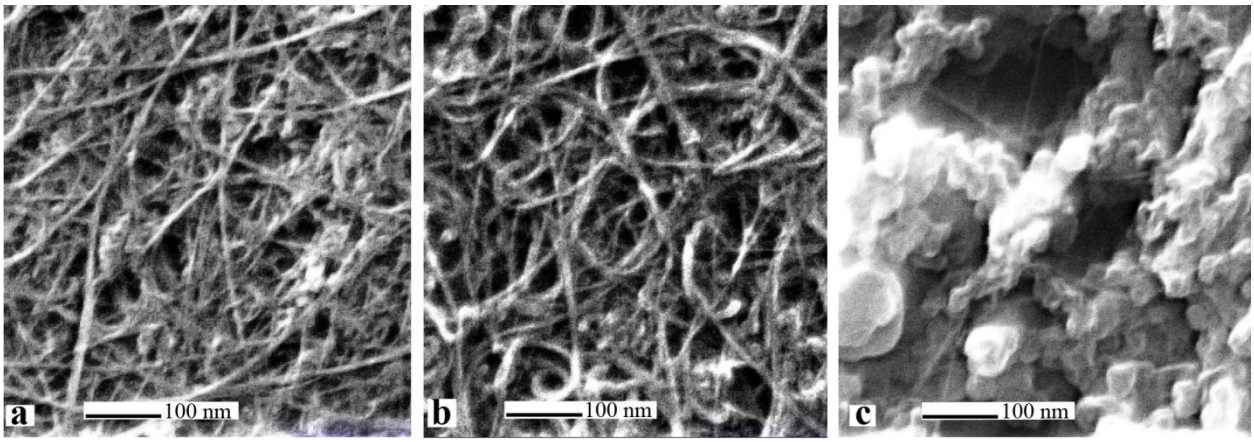

Figure 3.1 – SEM images of sp^2-carbon films at 130 000 X magnification: (a) a single-walled carbon nanotube film; (b) a mixed film consisting of single walled - multi walled carbon nanotubes (10 wt%-90 wt%); (c) a mixed film consisting of single walled carbon nanotubes and Ketjenblack™ carbon (20 wt%-80 wt%)

SWNT films were filtered from a 0.33 mg/ml CSA-dispersion (**Figure 3.1-a**). S-MWNT films were made from five CSA-dispersions with concentrations ranging from 0.33 to 1.67 mg/ml. The ratio SWNTs to MWNTs was 10 wt% to 90 wt% (**Figure 3.1-b**). SWNT-PC films were prepared from two dispersions with concentrations of 1.67 and 3.33 mg/ml, 20 wt% SWNT to 80 wt% PC (**Figure 3.1-c**). The resulting films had masses per unit area from 19.9 to 288 μg/cm^2. CNTs were purchased from Cheaptubes™ and used without further purification. These tubes were 1 to 2 nm in diameter, < 30 μm long, 99 wt% SWNTs, and < 8 nm diameter, < 30 μm long, 95 wt% for the MWNTs.

Using a Carver™ press, films were mated directly to 318-stainless steel metal current collector rods with different surface finishes: machined polished, roughened, and gold coated. Roughened rods were obtained by scratching machine polished rods with P100 aluminum oxide sand paper. Gold coated rods were produced by sputtering a ~20-nm thick layer of gold onto roughened rods. The pressure exerted between film and collector was 98 Mpa for all electrodes made. All rods were 1.2 cm-diameter cylinders that could be used directly in two-electrode type Swagelok™ cell. SWNT films and SWNT-PC

films were exclusively mated to gold coated collectors and S-MWNT films were cycled using all three collector surface finishes.

All cells were symmetrical full cells with identical electrodes (carbon film + current collector) on either side. Two different aqueous electrolytes were prepared: (i) potassium sulfate (K_2SO_4) dissolved at 0.5 mol/L (M) concentration in Milli-Q purified water with 18 MΩ.cm resistivity; (ii) concentrated 98% sulfuric acid (H_2SO_4) diluted in Milli-Q water until the concentration reached 0.5M. Fibreglass pre-filters from Millipore™ served as separators for all cells. They were soaked in electrolyte and placed between the electrodes.

Eighteen distinct cells were tested:

-One 19.9 μg/cm^2 SWNT-based cell mated to gold coated current collectors and 0.5M H_2SO_4 aqueous solution was used as electrolyte.

-Two SWNT-PC-based cells of two different carbon loadings (148.0 and 288 μg/cm2) mated to gold coated collectors, and with 0.5M K_2SO_4 aqueous solution as electrolyte.

-Fifteen S-MWNT-based cells with five different carbon loadings (22.4, 55.8, 88.2, 122.6, and 155.9 μg/cm^2) mated to all three types of collector. 0.5M K_2SO_4 aqueous solution was used as electrolyte.

3.2.2 Weighing

Accurate weighing is critical to the characterization of film performances: specific capacitance, current densities. The masses involved are also very small. The thinnest film weighing measured in at just over 109 μg. This film is about half the thickness of the thinnest film used in this work. The technique to make the film is to filter a controlled quantity of a sp^2-carbon suspension of known concentration. The reference suspension has a 3.33 g/L concentration. “ Film label in “ml” “ refers to this

reference solution. For instance a 0.5-ml film means that 0.5 ml of the 3.33 g/L suspension was filtered to form a film. Such a film should weigh $0.5 \times 10^{-3} \times 3.33 = 1.67$ mg. However, there is some loss occurring during filtering: some carbon passes through the filter itself because the pores are slightly bigger than the diameter of SWNTs, and also some carbon stays affixed to the filter when separation is done between carbon and filter. So the final film still needs to be weighed. The final weighing is done using a TA instrument Q600 thermogravimetric analyser with sub-micro gram accuracy. sp^2-carbon burns completely in air below 800 °C therefore it is easy to burn the sample and measure the differential in weight before and after burning to know the precise amount of carbon in each film.

For SWNT-AC films, the same weighing technique was employed however since only two thicknesses were needed, it was not possible to rely on a linear fit (**Figure S1**) between only two data points. Instead, four films were burned, two samples for each thickness and an average weight was taken for each film.

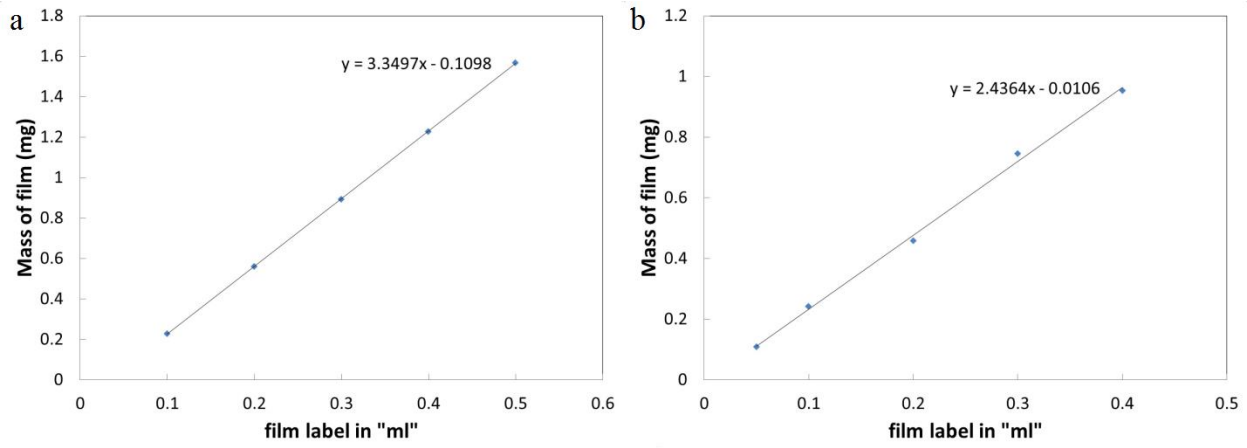

Figure 3.2 – Film weights: (a) Weight of 3.8-cm diameter SWNT-MWNT film disk of various thicknesses with linear fit; (b) Weight of 3.8-cm diameter SWNT film disk of various thicknesses with linear fit

3.2.3 Electrochemical measurements

Ruoff *et Al.* best practice methods were followed for measuring and deriving electrochemical properties of supercapacitors[54]. All cells were tested using a Biologic VMP3™ galvanostat and data was analyzed in EC-lab™ software. Galvanostatic tests were conducted with specific current values from 1 to 1460 A/g, between 0 and 0.8 V. Cyclic voltammetric test (CV) scan rates vary from 0.1 V to 1 kV/s, measurements above 200V/s are only qualitative as the galvanostat sampling frequency becomes insufficient for quantitative use above that sweep rate. Electrochemical impedance spectroscopy (EIS) measurements were conducted from 500 kHz to 100 mHz at a 5 mV amplitude with +0.1 V offset.

3.3 Results and discussion

3.3.1 Raman and FTIR characterisation

Thin films made from SWNTs were studied in comparison to raw SWNT powder to prove that the material had not undertaken any chemical or physical changes (functionalization). Raman tests reveal that both powder and film have similar peaks in amplitude and frequencies. The SWNT film itself, as well as raw SWNTs, were tested using FTIR technique to further confirm that there were no chemical change sustained by the nanotubes during their process into film. As expected, both samples film and raw powder revealed very similar outcomes whether they were tested through Raman or FTIR. Raman used a laser with frequency of 632.8 nm and it even shows that the film has a smaller D band peak than the powder. This may be explained by the elimination of remaining amorphous carbon from the powder by the chlorosulfonic superacid. Otherwise, FTIR measurements show very similar peaks for both powder and film demonstrating the non-damaging dispersion power of superacid.

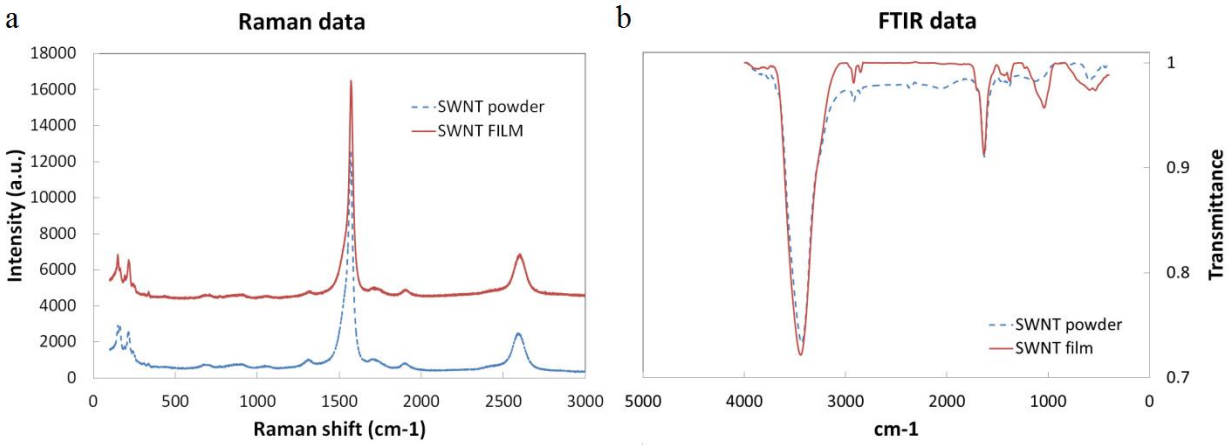

Figure 3.3 – CNT-powder & film Raman and FTIR characterisations: (a) comparative Raman spectra (632-nm laser) of pristine SWNT powder and film; (b) comparative FTIR spectra for pristine SWNT powder and film

3.3.2 Electrochemical impedance spectroscopy

From complex impedance representation, all fifteen S-MWNT cells displayed the same electrolyte (ionic) real impedance contribution: 0.36 Ω with a standard deviation of 0.04 Ω. This constant ionic contribution regardless of film thickness was proof of good ionic mobility through these CNT-films.

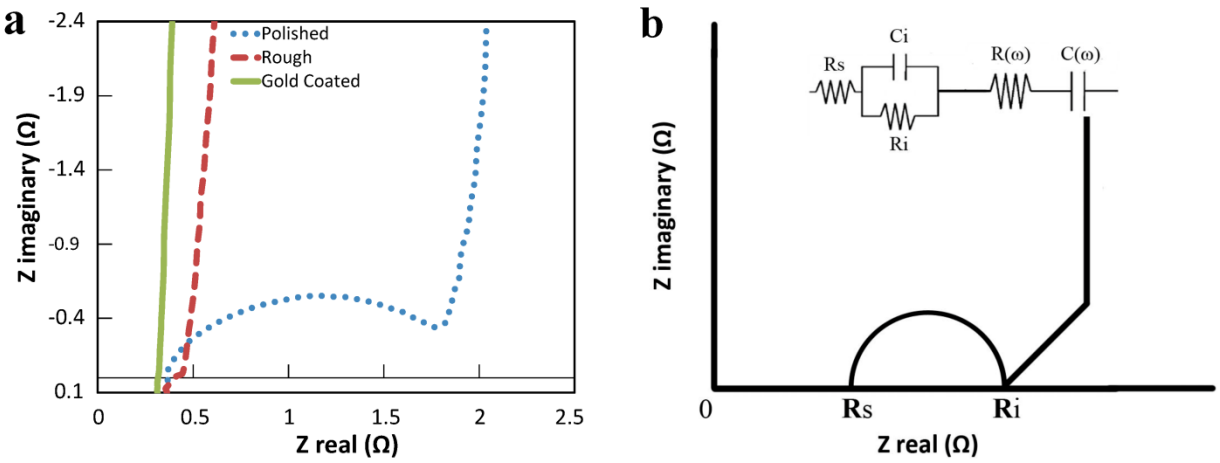

Figure 3.4 - Impedance spectroscopy of a single walled - multi walled carbon nanotube film (138 µg/cm^2; 0.5 M K_2SO_4) for polished, roughed and gold coated stainless steel current collectors: (a) complex plane impedance; (b) schematic showing equivalent circuit and complex plane impedance (R_s: solvent or ionic impedance, R_i: internal or electronic impedance, C_i: capacitance from contact resistance, R: additional resistance, C: EC capacitance))

Electronic impedance contributions differed significantly, however, depending on the choice of current collector as demonstrated with 138 µg/cm^2 films (**Figure 3.4**): 1.52 ± 0.07 Ω when the film is paired with polished collectors, 0.12 ± 0.02 Ω with roughened collectors, and a value not measurable through EIS with gold coated collectors. When carbon loadings were varied from 19.9 to 138 µg/cm^2 using identical current collectors, the electronic impedance increased from 0.15 to 1.52 Ω for polished collectors (**Figure 3.5-a**) whereas it did not change for gold coated collectors (**Figure 3.5-b**). This provides proof that electronic impedance was not generated inside the film but by the contact at the metal/carbon interface. These results are consistent with previous studies by Simon *et al.* on activated aluminum and on titanium/gold current collectors regarding the beneficial effects on conductivity arising from combining increased surface area from roughened surfaces with reduced oxide layer from metals like gold for current collectors[55, 56].

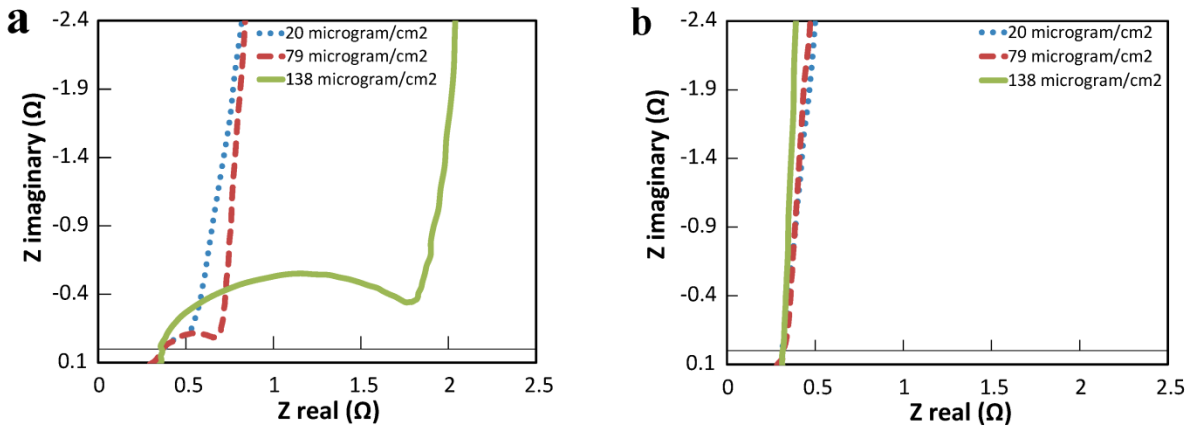

Figure 3.5 - Nyquist plots for single walled - multi walled carbon nanotube films: (a) comparison of different thicknesses of S-MW/NT-films on polished stainless steel collectors (b) comparison of different thicknesses of S-MW/NT-films on gold-coated stainless steel collectors

From the impedance data and assuming a resistor-capacitor in series configuration $\left(C = -\frac{1}{2\pi f Z_{Im}}\right)$, the 138 µg/cm^2-S-MWNT film coupled with gold coated current collectors yielded a RC-time constant of 1.06 ms and areal capacitance of 2087 µF/cm^2 at 120 Hz with -61° phase angle (**Figure 3.6**). Such phase angle value suggests non-negligible resistance behaviour for that electrode but it still provided an available capacitance that was seven times higher than the vertically-oriented graphene electrode made from electrochemically reduced graphene oxide and with similar time constant[45]. RC-time constants characterize every capacitor and are the results of charge mobility limitations, electronic and ionic, which appear as compounded resistance in series with the main capacitance. Therefore further reduction of the time constant must come from minimizing resistance if capacitance is to be kept large. Our 19.9 µg/cm^2-SWNT thin-film bonded to gold coated collector, cycled in a 0.5M H_2SO_4 electrolyte exhibited a proportionally much smaller 199-µs RC-time constant that was similar to Miller's vertically-oriented graphene electrodes but with over six times the capacitance[43, 45]. At 120 Hz, capacitance was 601 µF/cm^2 at -81°, and phase angle dropped to -45° at 1425 Hz (**Figure 3.6**). This represents a two-fold

increase in frequency response over the closest equivalent CNT-based device[57]. A summary of ultrahigh-rate capable aqueous supercapacitors and their performance is presented in **Table 1**. The performance displayed by our SWNT thin-film capacitor makes it suitable for AC-line filtering applications, where standard 60-Hz AC power is rectified to an all positive 120-Hz signal and then filtered to obtain direct current (DC) power. Its reduced 199-µs time constant provides access to more than 95% of the energy storage in the charge/discharge time given at 120 Hz.

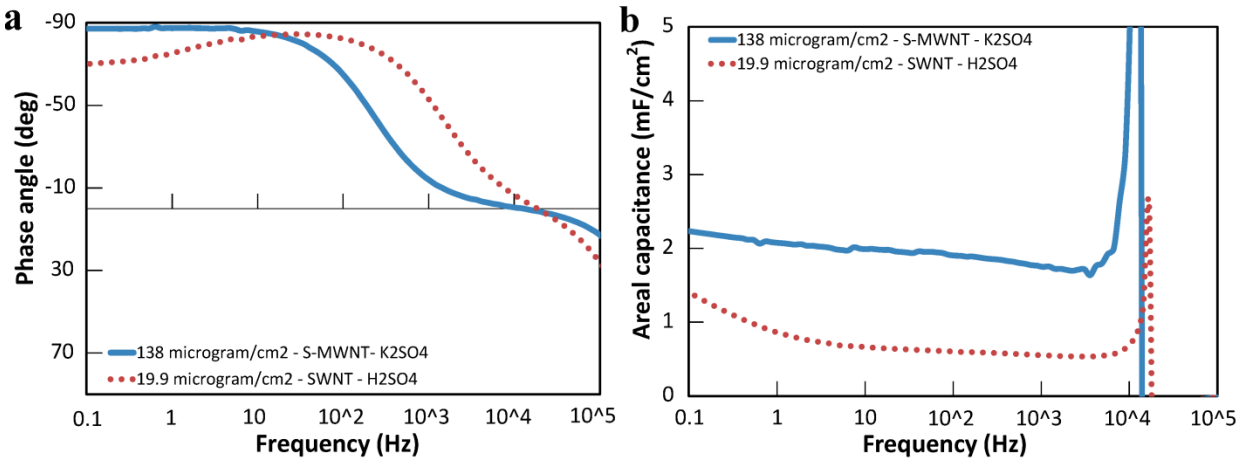

Figure 3.6 - Frequency response of S-MW/NT and SWNT films: (a) phase angle vs. frequency for a 19.9 µg/cm^2-SWNT film on a gold coated stainless steel electrode (0.5M H_2SO_4), and a 138 µg/cm^2-S-MW/NT film on gold coated electrode (0.5M K_2SO_4); (b) areal capacitance vs. frequency

3.3.3 Cyclic voltammetric

Cyclic voltammetric plots are presented on **Figure 3.7**. According to capacitance definition: C=q/V=I/(Sweep Rate), CV sweep rate remains proportional to current for an ideal constant capacitance. The 19.9 µg/cm^2-SWNT thin film mounted on gold coated collectors and cycled in a H_2SO_4 electrolyte supported CV sweep rates up to at least 200 V/s while maintaining direct proportionality between sweep rate and discharge current. A parallelepiped shape was maintained at 1 kV/s. This is faster than

any macro-sized CNT-based supercapacitor and second to Shi's graphene device which sustains proportional cycling sweep rates up to 350 V/s but these latter electrode exhibit much lower capacitance per unit area than CNT films[43, 58, 59, 60]. At the ultrahigh sweep rate of 200 V/s, discharge specific current reached 6400 A/g, which represents an extremely high response.

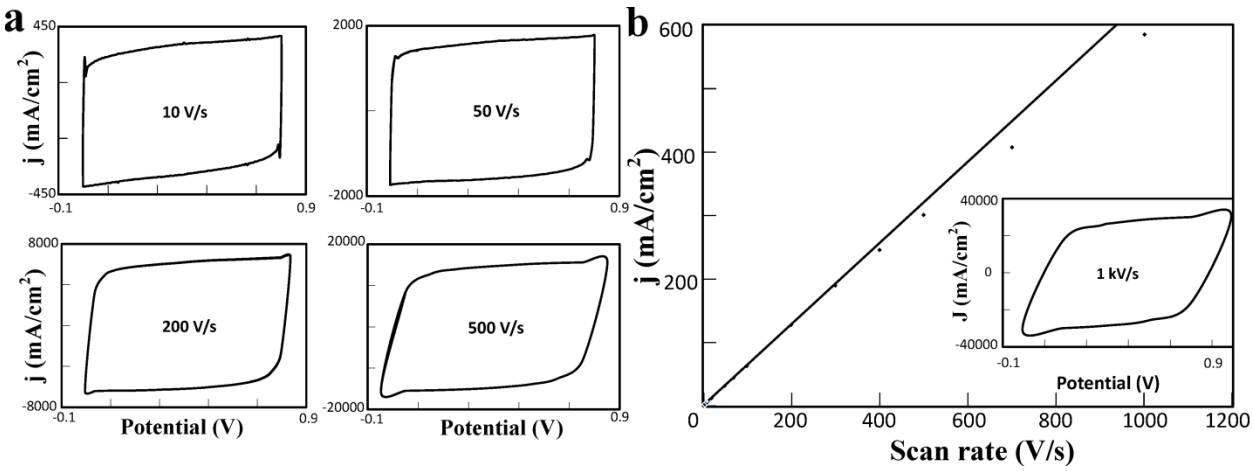

Figure 3.7 - Cyclic voltammetry studies of a 19.9 µg/cm^2-SWNT film on a gold coated stainless steel electrode (0.5M H_2SO_4) (a) CVs at scan rates ranging from 10 – 500 V/s; (b) discharge areal current versus scan rate showing onset of deviation from a linear response at 400 V/s; inset: CV at 1000 V/s

At 200 V/s, S-MWNT films mounted on gold collectors maintained quasi-constant specific current figures regardless of carbon loading, but the same films mounted on roughened and polished collectors did not. Constant current values at a given sweep rate indicated that nominal capacitance was reached. Electronic throughput through the collector surface area was found to reach a maximum of about 160 mA/cm^2 for cells using polished stainless steel collectors. Consequently that maximum limited current in the film bulk again singling out the carbon-metal interface as bottleneck for charge transfer (**Figure 3.8)**.

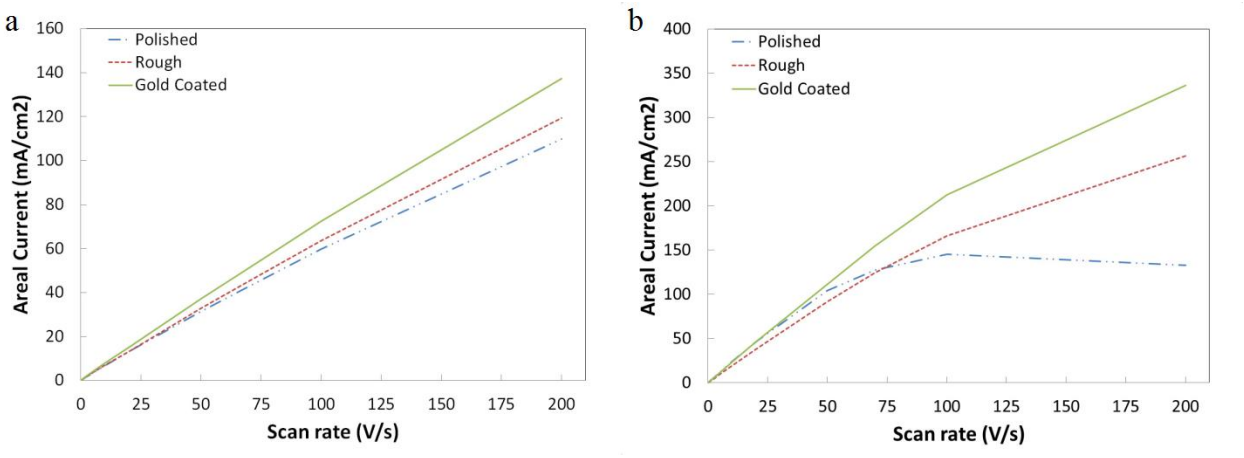

Figure 3.8 – Current response of S-MWNT films on different stainless steel current collectors: (a) scan rate current response for 49 µg/cm^2 film on polished, roughened and gold coated current collectors; (b) same as *(a)* for 138 µg/cm^2 film

3.3.4 Galvanostatic cycling

Figure 3.9 shows the capacitance loss when 138 µg/cm^2-S-MWNT-based cells were cycled from 1 to 100 A/g for 10 000 cycles. Losses tend to disappear for specific current values higher than 50 A/g. All S-MWNT and SWNT-PC cells could perform one million cycles with average capacitance loss of 1.4% (observed maximum of 2.5%). Impedance characteristics remained identical to pre-cycling values (**Figure 3.10**). Loss percentage figures were the same regardless of type of current collector used. Specific capacitance was measured at about 39 F/g for SWNT film, 33F/g for S-MWNT films and at 100 F/g for SWNT-PC films (**Figure 3.11**). Such maximum capacitance values are common for pure CNTs arranged in random networks[61].

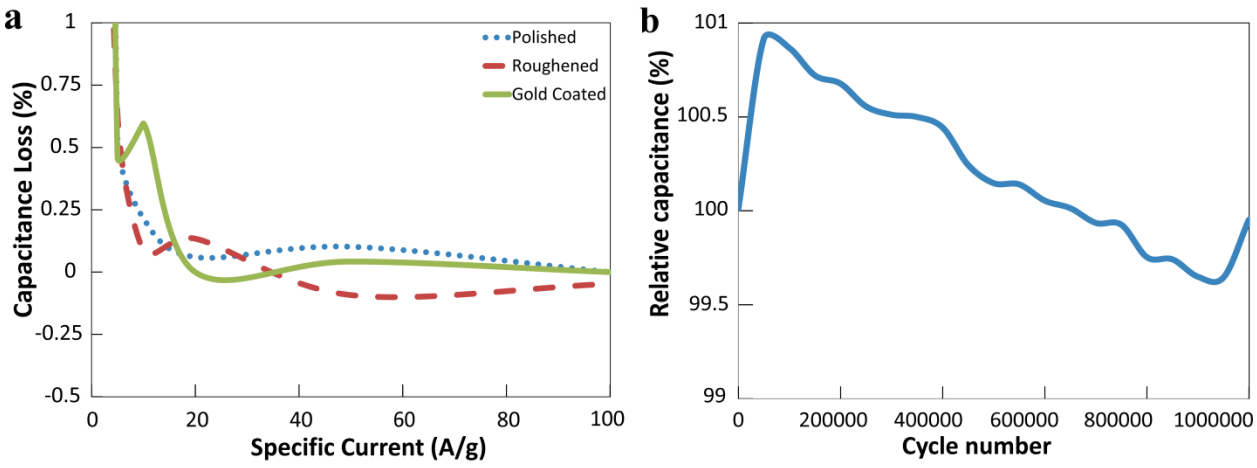

Figure 3.9 - Galvanostatic discharge tests of 138 µg/cm2 S-MW/NT films in 0.5M K2SO4 aqueous electrolyte: (a) capacitance loss vs. specific current for polished, roughened and gold coated stainless steel current collector; (b) plot of capacitance retention over one million cycle on gold coated collector when cycled at 200 A/g

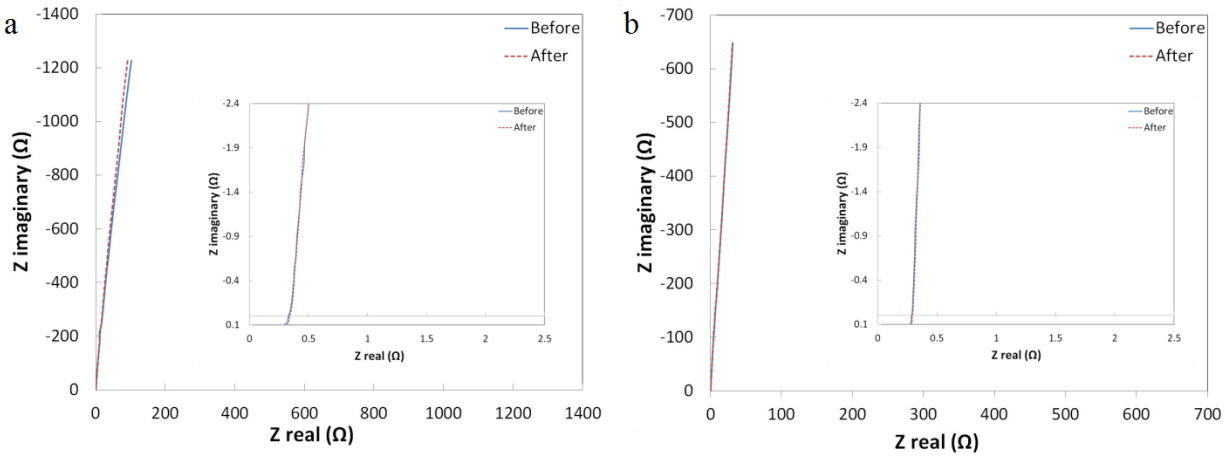

Figure 3.10 – EIS characterisation of S-MWNT films on gold current collectors: (a) Nyquist plot of complex plane impedance for 79 µg/cm^2 S-MWNT-film before and after 1 million cycle-run; (b) same as *(a)* for 138 µg/cm^2 S-MWNT film

It has been shown that capacitance contributions from surface functionalized groups decrease as cycle frequencies, that are proportional to specific current, increase past a few Hz[13]. Our carbons have not

been intentionally functionalized and this was verified using FTIR characterization (**Figure 3.3**). But some functionalized groups may form naturally from oxidation during production and even when carbon is left in storage in air. The observed dependence of capacitance loss on specific current values may then be explained by the suppression of pseudo-capacitance contributions from carboxyl or carboxylic groups at higher cycle frequencies.

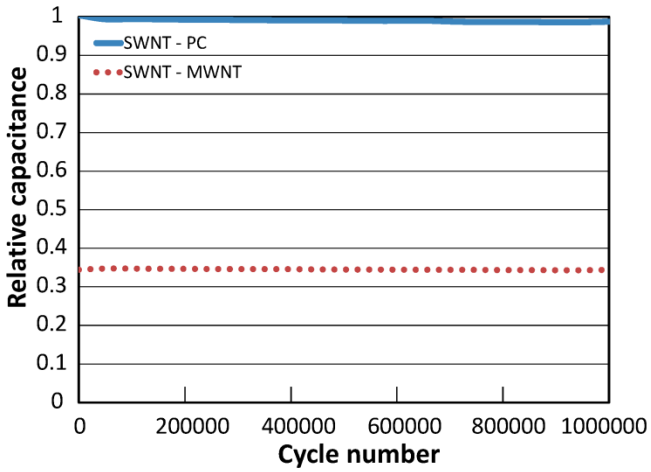

Figure 3.11 – Galvanostatic test of S-MWNT and SWNT-porous carbon films showing <98% capacitance retention after one million cycles at 200 A/g (143 ± 5 microgram/cm2; 0.5M K2SO4; gold coated stainless steel current collector)

3.3.5 Current collector surface characterization

To explain the differences in performance observed between current collectors, surface morphology and chemical composition were performed using a surface profilometer, atomic force microscopy (AFM), and x-ray photoelectron spectroscopy (XPS) At the microscale, surface roughness was characterized with a Dektak™ 8 Stylus contact profilometer. Across a 200-µm horizontal travel distance, polished surface shows typical maximum height Rz of 150 nm. Roughened and gold coated surfaces have greater and similar Rz values of 4750 and 6500 nm respectively (**Figure 3.12-a**). At the nanoscale, across a 1-µm horizontal travel distance, AFM study shows maximum heights of 9.4 and 11.0 nm for polished and roughened surfaces, and a typically greater height of 29.9 nm for the surface sputtered with gold. The different topography of the gold coated surface is imaged through scanning electron microscopy (SEM) and shows features in the tenths of nanometers range that are present all across the surface (**Figure 3.12-b**).

XPS analysis of chromium atom bond energies in stainless steel showed an increase oxidized chromium atoms on the surface of the roughened current collector compared to the polished collector. Atomic ratio of chromium oxide to chromium for the polished collector was calculated at 6.65 versus 25.2 for the roughened stainless steel surface. Chromium oxide on the polished surface was determined as being Cr_2O_3 whereas Cr_2O_3 and CrO_3 are present on the roughened surface (**Figure 3.12-c&d**). Whereas relative area increase between polished and roughened surfaces was estimated at just 1.008 times. We concluded that roughened stainless steel current collectors had at least the same thickness of non-conductive oxide on their surface than those that are polished.

It followed that the decreased electronic impedance and associated improvement in electronic charge transfer abilities obtained from roughened stainless steel over polished surfaces may be explained by an increase of actual contact area in the form of increased micro- and nano-scale friction. The number of

contact points between carbon and metal should increase with current collector roughness and therefore offer more pathways for electronic charges to flow between the two materials. The gold coated collector provides further improved electronic transfer through a combination of lack of metal oxide layer, confirmed by XPS study, to a further increase of number of contact points given by the nano-features imaged with SEM on its surface (**Figure 12-d**). These features size and morphology match the CNT-film porosity pressed on top of them and may offer an interlocked pairing configuration.

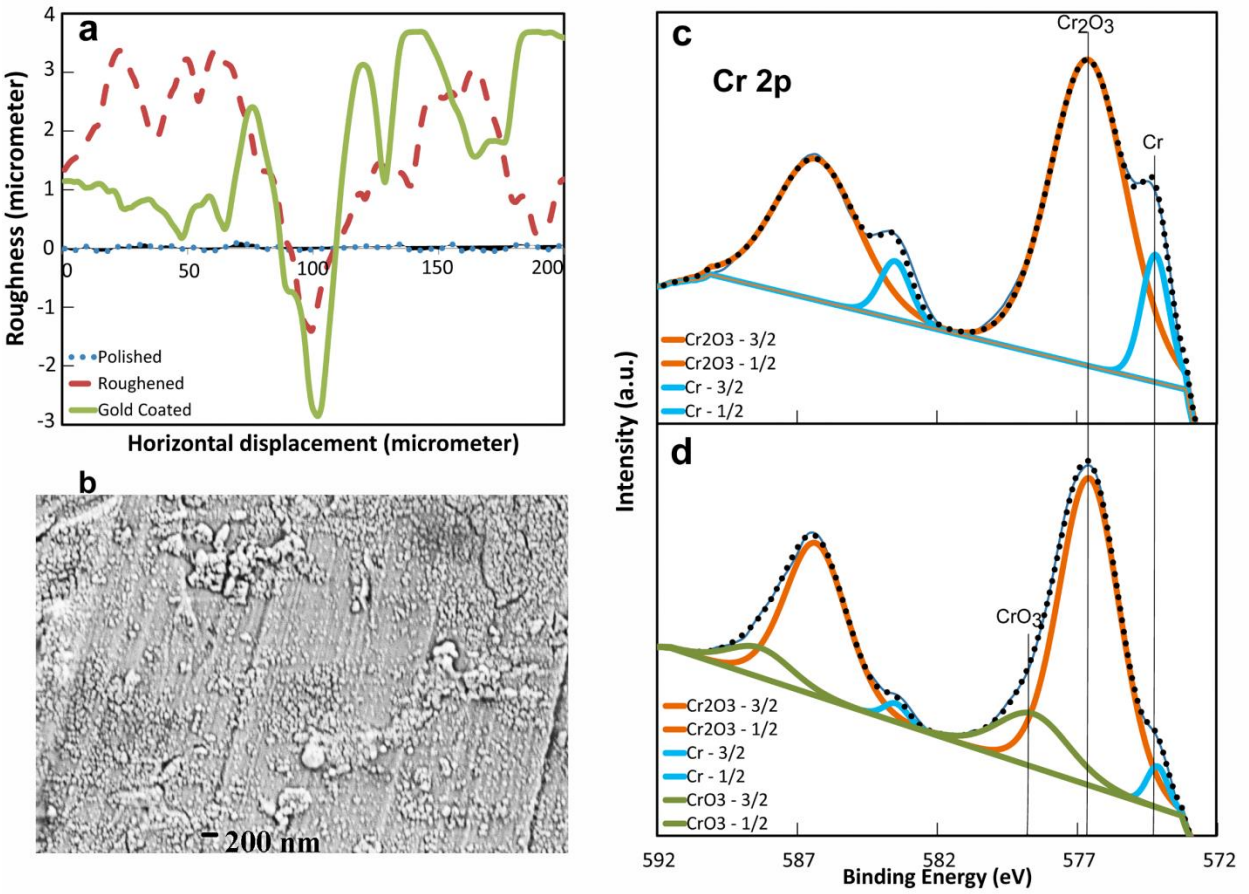

Figure 3.12 - (a) Comparative profilometry of polished, roughened and gold coated stainless steel current collector; (b) High magnification SEM image of gold coated collector showing nano-features on the surface roughened collector; XPS characterisation of chromium on: (c) polished stainless steel current collector (d) roughened stainless steel current collector

The graphene-based devices produced by Miller and Shi also exhibit electronic impedance contributions undetectable through EIS, but they present the highest frequency response reported for supercapacitors including the CNT-based devices present here (**Table 1**)[43, 45]. We believe that the direct growth and direct bounding used in Miller's and Shi's works are the key contributors to enabling fast cycling and especially high frequency responses as both construction methods lead to excellent effective contact at the interface of carbon and current collector, and prevents electrolyte from sipping between carbon and metal. Graphene has a more natural ability to form extensive contact with a relatively flat surface than carbon nanotubes due to its sheet morphology. Furthermore, Miller et al graphene is grown at 1000 °C directly on a nickel substrate in an inert atmosphere. This temperature is high enough to induce atomic inter-diffusion of carbon into nickel that would form very effective carbide channels for electrons to cross the carbon/metal interface[44]. However, chemical vapour deposition is unlikely to be a practical method for scaled up commercial production. Nevertheless, following Miller's lead, designs of energy storage devices may soon include bonding techniques developed decades ago in solar cell technologies where metal current collectors are bonded to active material through atomic diffusion for low resistance, energy efficient heterojunctions[62]. Contact of our electrodes relies on static friction between metal and CNT-bound films, thus explaining the slightly lower frequency response.

Table 3.1 – Comparison of high-rate capable supercapacitors and their performance metrics

	Max. Specific Capacitance *F/g*	Max. Areal Capacitance *μF/cm²*	Max. Scan Rate *V/s*	Frequency at -45° phase angle *Hz*	RC time constant @ 120 Hz *μs*	Areal Capacitance @ 120 Hz *μF/cm²*	Cycle Life	ESR *Ω/cm²*
Vertically grown graphene[43]	--	187.5	--	15 000	192.5	87.5	--	0.55
High density Vertically grown graphene[63]	--	--	--	30 000	251	94.8	--	1.65
Electrochemically reduced Graphene Oxide[45]	--	325	350	4 200	1 350	283	10 000 - no loss	1.13
Fibre-shaped EC reduced Graphene Oxide[64]	--	726	10	--	540	--	2000 - 6% loss	0.92
Carbon Onion micro-supercap.[58]	--	900	100	--	--	--	10 000	--
3D Graphene-CNT micro-supercapacitor[64]	--	2 160	400	500 to 1 300	195 to 402	230 to 662	--	380 to 553
On-chip CNT supercapacitor[49]	--	200	2000	450	--	--	--	0.16
Electrophoretic deposited CNT[57]	21	--	1	~600	--	--	--	1.17
CNT-sponge supercapacitor[26]	3.75	900	8	--	--	--	100 000 - 2% loss	~6
Carbon black thin film on vinyl[65]	--	--	--	641	354	559	--	0.3
Carbon black thin film by inkjet printing[65]	--	500	--	764	588	120	--	4.9
SWNT	**27**	**600**	**200**	**1 425**	**199**	**601**	**--**	**0.25**
S-MWNT	**33**	**2 300**	**100**	**223**	**1 060**	**2 087**	**1 million - <2%**	**0.3**
SWNT-PC	**100**	**11 500**	**20**	**--**	**--**	**--**	**1 million - <2%**	**0.35**

3.4 Conclusion

In this chapter, the rate capability of well-known sp^2-carbon compounds have been demonstrated to be at least two orders of magnitude higher than previously reported: 2000 A/g for SWNT-PC films, 2400 A/g for S-MWNT films, and 6400 A/g for SWNT films. These high specific currents areenabled by the self-assembly of CNTs into extremely conductive flexible mesoporous networks when previously filtered from CSA dispersions, their ability to bind other sp^2-carbons, and through the use of tailored current collectors[51]. These electrodes compete well with graphene-based supercapacitors, displaying low interfacial resistivity, higher areal capacitance, and high cycle life. AC-line filtering applications are within reach of CNT-based supercapacitors. I have also demonstrated that, for mesoporous electrodes with un-impaired ionic transport abilities, limitations came from electronic transfer through the carbon/metal interface as the high electronic specific currents that are possible inside carbon can overwhelm the ability of metal/carbon interfaces to transfer electrons from the carbon to the current collector. The versatile construction method presented isolate the role of current collectors as a significant bottleneck for charge transport in electrodes with otherwise unrestricted currents. It also helps demonstrate the importance of increasing the number of contact points between active material and metal current collector. In this chapter effective contact points were varied through different surface roughness. Other morphologies at the micro- and nano-sized may be even more effective like 2-D materials. Finally it is clear that better interface conductivity is still a key component in future developments of high-power energy storage devices.

CHAPTER 4 – COMPOSITE CARBON NANOTUBE-Ti_2C MXENE FILM FOR HIGH-CURRENT CAPABLE PSEUDO-INTERCALATION OF CATIONS FOR SUPERCAPACITORS

4.1 Introduction

Mxene materials have relatively low surface area but they can provide specific electrochemical capacitance on par with high surface area materials like porous carbons. Charge storage in Mxene material derives from pseudo-intercalation of cations in-between Mxene sheets. Because of this mechanism and the relatively high density of the material, volumetric capacitance is much higher than what is achievable with carbon; values of 300 F/cm^3 have been reported for Ti_2C in 2013 by Gogotsi *et al*. Ti_2C Mxene is a conductive material with a two-dimensional sheet morphology similar to that of graphene. This characteristic motivated us to make a composite material with the incorporation of carbon nanotubes (CNTs). CNTs could prevent ion transport blockage between Mxene particles. The stacking up of sheet like materials lead to reduced available surface area and loss of capacitance at high sweep rates[45]. Pure Mxene electrodes rely on a balance between sheet-to-sheet direct contact for good electron conductivity, and sufficient separation between sheets for ion transport. Introducing single walled nanotubes as a spacer would eliminate this compromise and allow for higher loading per unit surface area with higher volumetric capacitance and minimal obstruction of ion movements.

The conduction properties of CNTs would increase bulk conductivity of the composite material by providing efficient electronic conduction channels between adjacent sheets of material. In addition, Van der Waals forces between CNTs and Mxene would allow for the making of self-standing films. Finally, contrarily to Mxene materials, CNTs are hydrophobic. That will prolong the integrity of composite electrodes when aqueous electrolytes are used.

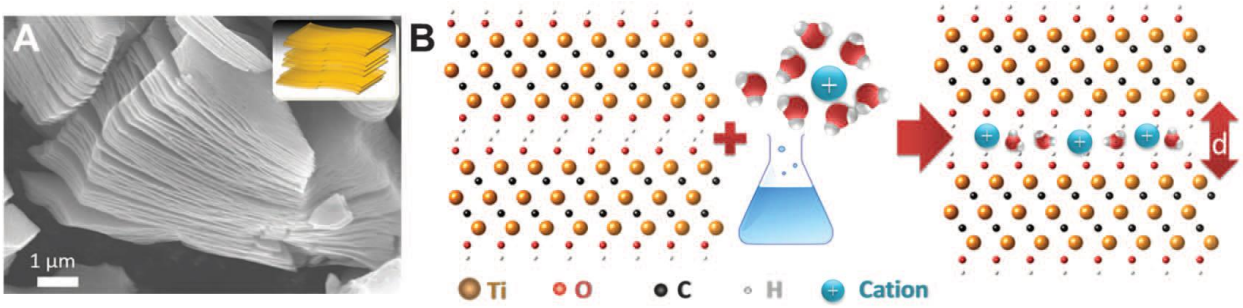

Figure 4.1 – (a) Scanning electron microscopy (SEM) picture and (b) schematic of pseudo-intercalation material from reference 9

Pseudo-intercalation as a supercapacitive charge storage mechanism is relatively new and previous efforts have only reported cycling under a relatively low specific current of 1 A/g[9]. In this chapter, we present the construction of composite CNT-Ti_2C electrodes from exfoliated and non-exfoliated materials; both present enhanced electronic and ionic transport abilities. These electrodes are made with either larger particles of non-exfoliated Mxene material or smaller exfoliated sheets. The aim of this study is to illustrate the effect of particle size on pseudo-intercalation charge storage at high specific currents up to 100 A/g. Finally, the contact quality at the active material/current collector interface is investigated and compared to pure CNT electrodes from Chapter 3.

Guidance on Mxene material synthesis, processing and x-ray diffraction (XRD) characterisation from Dr. Xiao Liang is acknowledged.

4.2 Experimental

4.2.1 Binder-free Mxene films, electrode and cell preparation

Ti_2C Mxene was produced from etching aluminum out of Ti_3AlC_2 MAX phase powder in hydrofluoric acid (HF) in a procedure derived from a previously reported method[9].

Purchased MAX phase was dispersed in 10% Hydrofluoric acid (HF) solution and stirred for 10 hours in a plastic container. The resulting solution was centrifuged in plastic tubes at 11000 rpm for 10 minutes in order to separate the Mxene phase from liquid HF solvent. The powder is then washed and centrifuged with water three additional times. The product is finally dried overnight at 90 °C to obtain non-exfoliated Ti_2C Mxene phase.

DMSO treatment. As previously reported, Mxene can be exfoliated by dispersing it in dimethyl sulfoxide (DMSO). Our exfoliation technique is derived from the originally reported method by Gogotsi[9]. Non-exfoliated Ti_2C Mxene powder is dispersed in DMSO and stirred for a minimum of 18 hours. Exfoliation is realized via intercalation of solvent molecule in-between the sheet structure. To complete the exfoliation process and reduce particle size, the dispersion is sonicated with a high-powered QSONICAM-Q500™ tip sonicator. The sonicator is programmed to produce 5-second pulses separated with 2-second pauses. The amplitude of the tip movement is limited to 30% of maximum deflection. Three 5-minute cycles are performed for a total time of 15 minutes of sonication. This procedure keeps the dispersion at a temperature manageable for handling. After sonication, the dispersion is centrifuged at 11000 rpm for 10 minutes to separate Mxene from DMSO. Mxene is then dispersed in water. The aqueous suspension is again sonicated with the tip sonicator in identical pulse mode but with 40%

amplitude. The sonication is then carried out in two 5-minutes steps to prevent the aqueous solution from boiling. Finally the dispersion is centrifuged at 2500 rpm for 6 minutes to help larger particles crash out of solution. Filtration through a polycarbonate membrane filter with 200 nm pores is performed next followed by overnight drying at 90 °C. Once dried, Ti_2C Mxene is finally dispersed in chlorosulfonic acid at a concentration of 16.67 g/L. The acid dispersion is stirred overnight.

Composite films were made by mixing dispersions of single walled carbon nanotubes (SWNTs) and Mxene following the same procedure described in Chapter 3. Four composite films are produced, each containing 0.8 mg/cm^2 of exfoliated or non-exfoliated Mxene with varying weight percentages of SWNTs:

- Three films are made with 0.8 mg/cm^2 of non-exfoliated Ti_2C; these films contain 2.4, 7 and 18 wt% of SWNTs respectively.
- Three films are made with 0.8 mg/cm^2 of exfoliated Ti_2C; these films also contain 2.4, 7 and 18 wt% of SWNTs respectively.
- One Ti_2C 0.8 mg/cm^2 film is deposited directly on a glass-fibre separator.

Cells are in two- and three-electrode configurations. Two-electrode cells are symmetrical. Three-electrode cells use a 3M Ag/AgCl reference electrode and a composite carbon film as counter electrode. This counter electrode weighs approximately 1 mg/cm^2 and is made of 20 wt% SWNTs and 80wt% ketjen black. All films are mated to roughened stainless steel again in the same manner we described in Chapter 3.

4.2.2 Electrochemical measurements

Electrochemical measurements are conducted identically as reported in Chapter 3 except for the following:

- Galvanostatic tests are carried out with currents ranging from 1 to 400 A/g. Cyclic voltammetry tests (CV) are conducted on three-electrode cells from -0.6 to 0V versus an Ag/AgCl reference electrode.

- CV sweep rates vary from 0.01 to 1 V/s.

- Electrochemical impedance spectroscopy tests (EIS) are conducted on two-electrode cells from 500 kHz to 100 mHz at a 5 mV amplitude with no direct current offset.

4.3 Results and discussion

4.3.1 X-ray diffraction (XRD) characterisation

Mxenes are a family of materials with good chemical inertness. Nevertheless, because of their recent discovery, experimental data on this subject is sparse. For the purpose of our experiment, electrode material needs to be well dispersed and carbon nanotubes have to be incorporated to the dispersion in order to produce a homogeneous, self-standing, conductive film. We elected to utilize the same dispersant that was successfully used with sp^2-carbons in Chapter 3: chlorosulfonic acid (CSA). Our main investigation of Ti_2C Mxene dispersed in CSA involves comparative XRD spectra. XRD peak shifts would indicate that the material had undergone some reaction with the acid. Incorporation or removal of atoms in the crystalline structure would most likely change inter-planar distances that would produce peak shifts in XRD spectra. **Figure 4.2** shows an almost exact superposition of spectra obtained before and after acid dispersion. This is a strong indication that Ti_2C has remained unaffected by CSA.

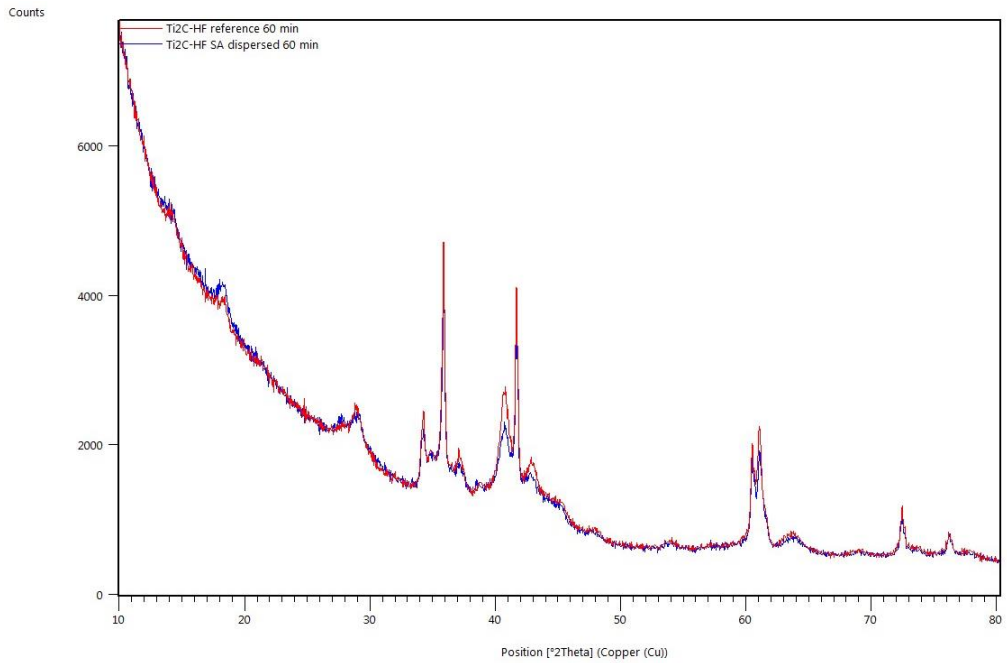

Figure 4.2 – XRD comparative plot of Ti_2C Mxene before (red trace) and after (blue trace) dispersion in chlorosulfonic acid

4.3.2 Galvanostatic cycling

From reference 9, the pseudo-intercalation charge mechanism of Ti_2C Mxene have been shown to produce about 70 F/g of specific discharge capacitance when the material is intercalating potassium (K^+) cations from an aqueous electrolyte. This capacitance is stable and it is maintained over 10000 cycles. **Figure 4.3** shows equivalent capacitance for our pure acid dispersed Mxene film at 2 A/g and higher. Composite films that include CNTs as conductive binder all feature superior values of capacitance even up to 100 A/g. Capacitance for composite films remains stable over 10000 cycles (**Figure 4.3-b**). This experiment provides additional evidence that the charge storage mechanism of CNT-Ti_2C composite films is the same pseudo-intercalation mechanism reported by Gogotsi *et al*[9].

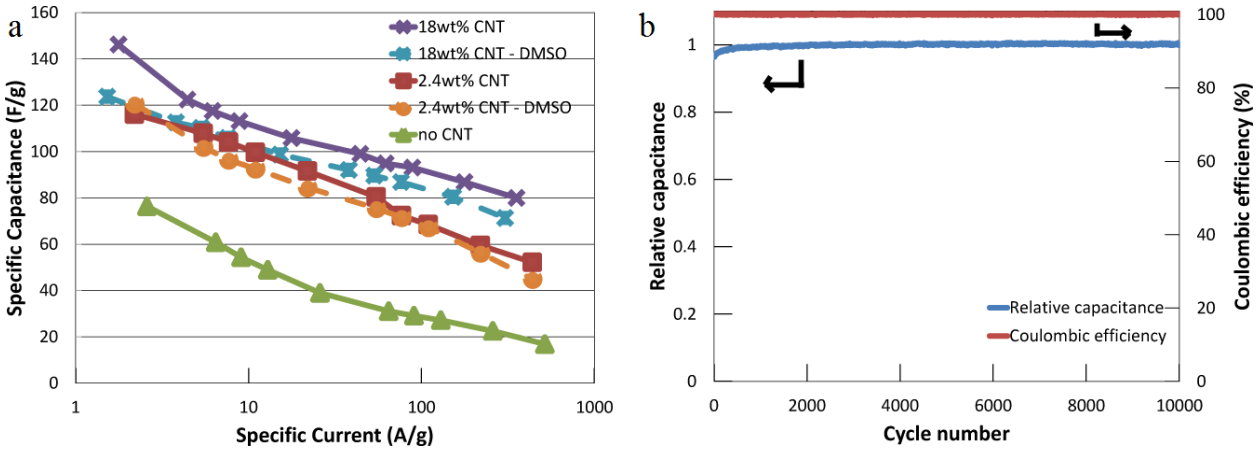

Figure 4.3 - Galvanostatic cycling of CNT-Mxene films in 0.5 M K_2SO_4 aqueous electrolyte: (a) specific capacitance of Mxene and CNT-Mxene composite films with 0.8mg/cm^2 at different specific currents; (b) capacitance retention for 2.4wt% CNT-exfoliated Ti_2C film over 10000 cycles when cycled at 70 A/g

The addition of CNTs provides both a clear increase of specific capacitance as well as capacitance retention at higher specific discharge current. As the amount of CNTs is increased, capacitance retention at high currents becomes consistently greater. It is worth noting that at 18 wt%, CNTs double layer charge storage contributes less than 6% of the overall capacitance. Meanwhile overall capacitance is increased by more than 30% for films containing non-exfoliated Ti_2C at specific current higher than 100 A/g. We conclude that pseudo-intercalation benefits from the added electronic conductivity provided by the nano-contacts formed by CNTs entangled with Mxene.

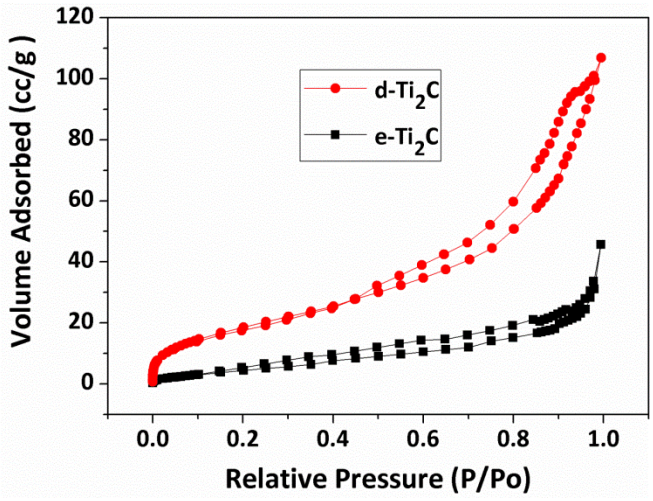

Figure 4.4 – BET adsorption data comparison between non-exfoliated Ti_2C (black) and DMSO treated Ti_2C (red)

Exfoliated Mxene under-performs when compared to the non-exfoliated variety despite its higher surface area measured in BET (**Figure 4.4**). This might be explained by film density. Exfoliated Mxene sheets allow for a much more compact film at 696 mg/cm^3 compared to 264 mg/cm^3 (**Figure 4.5**). Volumetric capacity grows from 294 to 746 F/cm^3 for exfoliated material when cycled at 4 A/g. High film density is produced by adding CNTs to small exfoliated Mxene sheets (<100 nm). It has been reported that graphene, that is also a 2D material like Mxene, tend to obstruct ion path when sheets are stacked up[45]. We believe that compromised ionic transport and partially inaccessible material explain the lower capacitance observed for exfoliated material when compared to non-exfoliated material.

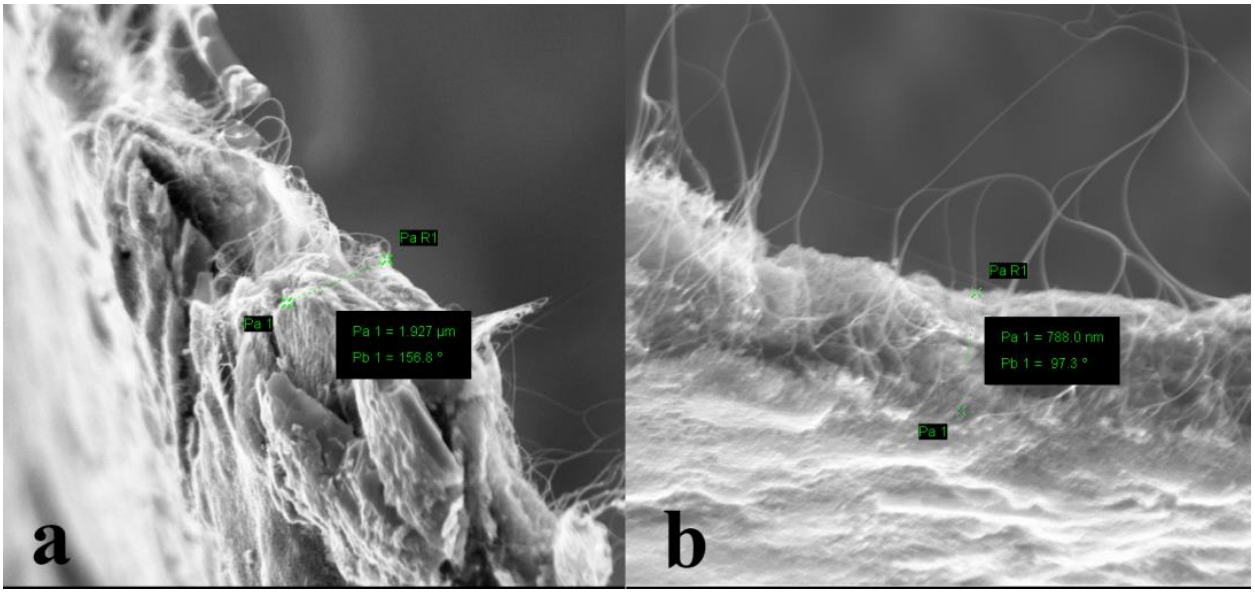

Figure 4.5 – SEM images of CNT-Ti_2C with 0.4 mg/cm^2 of Mxene: (a) 0.51mg/cm^2 film from HF treated maxene exhibits a thickness of 1.93 µm; (b) 0.55mg/cm^2 film from HF + DMSO treated maxene exhibits a thickness of 0.79 µm

4.3.3 Cyclic voltammetric

Cyclic voltammetric tests confirm results obtained through galvanostatic cycling. Pure Mxene electrodes lose significant capacitance at 100 mV/s and higher. That loss is effectively mitigated with the addition of CNTs as displayed by the composite films which retain most of the original capacitance up to 1 V/s. Again higher the CNT content produces better performance under the high currents that come with the higher sweep rates (**Figure 4.5**).

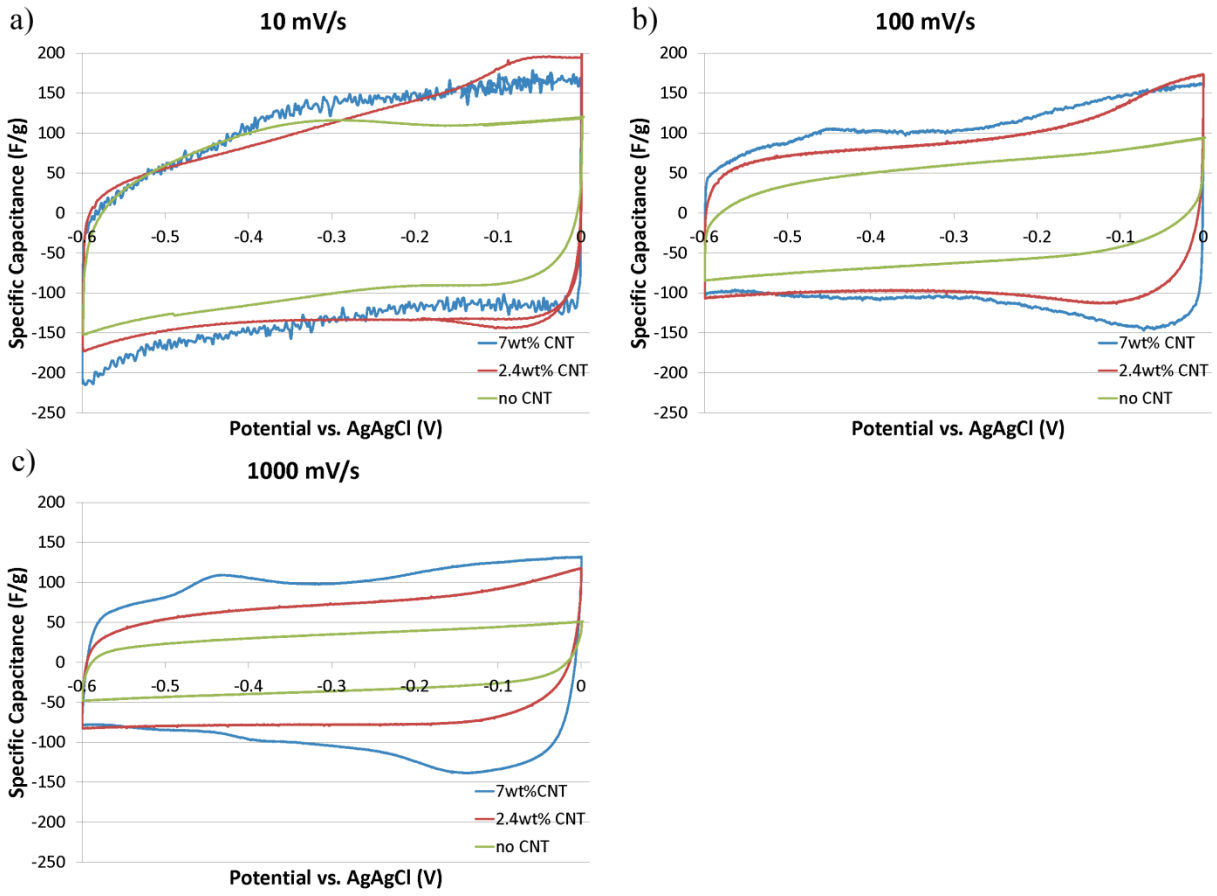

Figure 4.6 – Cyclic voltammetry tests of electrodes containing 0.8mg/cm^2 of Ti_2C with 7wt%, 2.4wt% and no CNT added cycled on roughened stainless steel current collectors in 0.5M K_2SO_4 at: (a) 10 mV/s, (b) 100 mV/s, (c) 1000 mV/s

4.3.4 Electrochemical impedance spectroscopy

From the EIS spectra, composite Mxene films all produce very low overall series resistance (<0.4 Ω/cm^2) when paired to roughened stainless steel current collectors. This value is equivalent to a pure CNT-film mated to the same current collector (**Figure 4.6**). However, Nyquist plots reveal a lower electrical resistance contribution for composite Mxene films compared to pure CNT films. Electronic contribution is 0.05 ± 0.01 Ω for composite CNT-Ti_2C films and 0.12 ± 0.02 Ω for comparable CNT-film.

On Nyquist plots, initial crossings with the real impedance axis for all films occur within 0.36 ± 0.04 Ω range (cf. **Figure 4.7**). This range corresponds to the experimental error determined in Chapter 3 for ionic impedance. We conclude that, within experimental errors, ionic impedance is the same for CNT and CNT-Ti_2C exfoliated and non-exfoliated films. Furthermore, as shown in Chapter 3, CNT-films do not have noticeable bulk electronic impedance leaving the observed electronic impedance entirely to contact resistance at the metal/film interface. Therefore, it can be safely concluded that composite Mxene films form much lower contact impedance when paired with metal current collectors than CNT films. Since Mxene is a 2-D material, this result confirms the assumption that a 2-D material morphology would produce more effective contact points through which electrons can flow across an interface. The natural ability of nano-sheets to conform at the nano-level to a surface that is mostly flat most probably produces more contact points between film and metal.

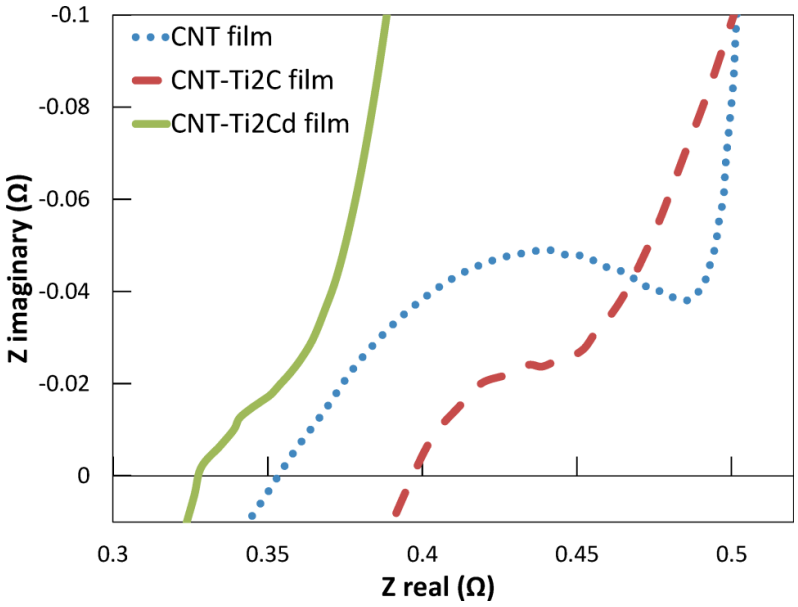

Figure 4.7 – High frequency EIS spectra of CNT-Ti_2C film exfoliated (green) and non-exfoliated (red), and pure CNT film (blue) tested with roughened stainless steel current collectors in 0.5M K_2SO_4

4.4 Conclusion

In this chapter, Mxene have been shown to be dispersible in chlorosulfonic acid with no effect on either inter-planar crystalline distances or the cation intercalation mechanism. From this homogeneous suspension, composite CNT-Ti_2C Mxene films have been produced. The addition of single walled carbon nanotubes considerably increased performance from pseudo-intercalation charge storage mechanism by maintaining 90 F/g under specific current over 100 A/g. The CNT-Ti_2C electrodes are also able to maintain nearly identical specific capacitance from 10 mV/s to 1 V/s. These results are attributed to better charge transport provided by the incorporation of pristine CNTs. Exfoliated Ti_2C materials, with particle size reduced through high-power sonication, produced compact films with the highest reported volumetric capacitance 746 F/cm^3 for any Mxene material. Finally 2-D Mxene composite films out-performed pure CNT films in forming electronically conductive interface contacts with stainless steel current collector confirming the assumption formulated in Chapter 3. This study provides proof that interfacial resistance can be reduced through the creation of a greater number of effective contact points as an alternative to using gold coated current collector for high current throughput.

Future perspectives

The work presented in this thesis has been focused on improving charge transport inside active materials through the use of carbon nanotubes. It was proven that both double layer and pseudo-intercalation charge storage mechanisms can be made to cycle two orders of magnitude faster than previously reported opening up new applications for supercapacitor technology like AC-line filtering. It was also shown that there is a critical bottleneck at the current collector interface and that great improvement can be obtained by designing more effective and numerous conductive contact points at this particular interface. At least an additional two orders of magnitude in frequency response can be expected from doing such work. Carbon nanotubes used as electrode binder enables very high current per mass of total active material, maintaining electrical contacts between particles and with current collectors. The work presented in this thesis demonstrates that electronic contacts at the micro- and nano-level are highly dependent on morphology and can be greatly improved by changing the shape of contacting materials. However the electrical connection they provide are only through surface contacts that are maintained by weak secondary forces. Furthermore, charge storage mechanisms like double layer formation, or cation pseudo-intercalation are only limited by charge transport phenomena. Therefore these supercapacitive systems shall still support and take advantage of higher currents and higher drive frequencies. Studies on single carbon nanotubes contact with metal have demonstrated that conductivity is improved by either using intermediate compounds that increase the “wetting” of nanotubes or by heat treatments[66 67]. Published work on vertically aligned graphene sheet with carbon atoms that accidently diffused inside a nickel current collector already present higher performance than similar electrodes with no carbon diffusion proving that supercapacitors benefit from improved electronic conductivity[44, 45].

Future work involving the active material/current collector interface may include vacuum brazing of CNT electrodes or CNT composite electrodes binding other types of active materials to ordinary aluminum or copper current collectors[68]. Intermediary conductive pastes containing silver nanoparticles can be also placed in-between active material and the metal to increase contact area[69]. Finally high-temperature diffusion of carbon active material under vacuum or reducing atmospheres may be used to produce a chemically bonded carbide interface as well as creating bonds between active material particles and CNTs. This last option is the most promising but requires specially selected metals that would produce chemically inert and conductive carbides like titanium or nickel.

Supercapacitors are very similar to the much more popular lithium batteries; sharing a common architecture and even electrode materials and technologies but supercapacitors have much simpler chemistries which make them a much more tractable bench work for researching the effects of architectural changes on charge transport. Less reactive chemistries and simpler mechanisms give greater freedom in choosing materials, creating chemical bonds. Also heating tolerances are higher and more chemical treatment avenues can be followed without damaging the simpler charge storage mechanisms of supercapacitor electrodes compared to lithium battery electrodes. But in the end, all electrical storage solutions including lithium batteries may benefit from improved interface conductivities obtained in supercapacitor developments. Improved conductivity translates directly into increased performance and energy efficiency. Electric cars nowadays are range limited and yet still lose part of the stored energy through heat wasted in on-board cooling systems. At the date of this thesis submission, all electric energy storage systems, including popular lithium batteries, rely on surface contacts for electrical conductivity. Therefore researching novel, advanced, nano-electronic connections relying on the primary forces of atomic bonds has a large breadth of potential applications and may be immensely useful for electrical energy storage systems and applications.

References

[1] Martin C., *Driving change in the battery industry*, Nature Nanotechnology (2014) 9, 327-328

[2] Miller J. R., Burke A. F., *Electrochemical Capacitors: Challenges and Opportunities for Real-World Applications*, The Electrochemical Society Interface (2008) 53-57

[3] Ho M. Y., Khiew P. S., Isa D., Tan T. K., *A Review of Metal Oxide Composite Electrode Materials for Electrochemical Capacitors*, NANO: Brief Reports and Reviews (2014) 9, 6, 1430002

[4] Yu A., Davies A., *Material Advancements in Supercapacitors: From Activated Carbon to Carbon Nanotube and Graphene*, The Canadian Journal of Chemical Engineering, (2011) 89, 1342-1357

[5] Jiang H, See Lee P., Li C., *3D carbon based nanostructures for advanced supercapacitors*, Energy & Environmental Science, (2013) 6, 41-53

[6] Simon P., Gogotsi Y., *Materials for electrochemical capacitors*, Nature Materials (2008) 7, 845-854

[7] Kim T.Y., Jung G., Yoo S., Suh K., Ruoff R., *Activated Graphene-Based Carbons as Supercapacitor Electrodes with Macro- and Mesopores*, ACS Nano (2013) 7, 8, 6899-6905

[8] Augustyn V., Come J., Lowe M., Kim J., Taberna P., Tolbert S., Abruna H., Simon P., Dunn B., *High-rate electrochemical energy storage through Li^+ intercalation pseudocapacitance*, Nature Materials (2013) 12, 518-522

[9] Lukatskaya M., Mashtalir O., Ren C., Dall'Agnese Y., Rozier P., Taberna P., Naguib M., Simon P., Barsoum M., Gogotsi Y., *Cation Intercalation and High Volumetric Capacitance of Two-Dimensional Titanium Carbide*, Science (2013) 341, 1502-1505

[10] Simon P., Gogtsi Y., *Charge storage mechanism in nanoporous carbons and its consequence for electrical double layer capacitors*, Philosophical Transactions of the Royal Society A (2010) 368, 3457-3467

[11] Chmiola J., Yushin G., Gogotsi Y., Portet C., Simon P., Taberna P.L., *Anomalous Increase in Carbon Capacitance at Pore Sizes Less Than 1 Nanometer*, Science (2006) 313, 1760-1763

[12] Gogotsi Y. ,Nikitin A., Ye H., Zhou W., Fischer J. E., Yi B., Foley H. C., Barsoum M. W., *Nanoporous carbide-derived carbon with tunable pore size*, Nature Materials (2003) 2, 591-594

[13] Segalini J., Iwama E., Taberna P.L., Gogotsi Y., Simon P., *Steric effects in adsorption of ions from mixed electrolytes into microporous carbon*, Electrochemistry Communications (2012) 15 63-65

[14] Ji H., Zhao X., Qiao Z., Jung J., Zhu Y., Lu Y., Zhang L., MacDonald A., Ruoff R., *Capacitance of carbon-based electrical double-layer capacitors*, Nature Communications (2014) 5, article number 3317

[15] Black J. ,Andreas H. A., *Effects of charge redistribution on self-discharge of electrochemical capacitors*, Electrochemica Acta (2009) 54, 3568-3574

[16] Andreas H. A., Lussier K., Oickle A., *Effect of Fe-contamination on rate of self-discharge in carbon-based aqueous electrochemical capacitors*, Journal of Power Sources (2009) 187 275-283

[17] Beguin F., Presser V., Balducci A., Frackowiak E., *Carbons and Electrolytes for Advanced Supercapacitors*, Advanced Materials (2014) 26, 2219-2251

[18] Fic K., Lota G., Meller M., Frackowiak E., *Novel insight into neutral medium as electrolyte for high-voltage supercapacitors*, Energy & Environmental Science (2012) 5, 5842-5850

[19] Ratajczak P., Slesinski A., Jurewicz K., skowron P., Frackowiak E., Beguin F., *Gas evolution and accompanying reactions contributing to the deterioration of electrochemical capacitors in salt aqueous electrolyte* POSTER at ISE meeting (2014)

[20] Zhu Y., Murali S., Stoller M. D., Velamakanni A., Piner R. D., Ruoff R. S., *Microwave assisted exfoliation and reduction of graphite oxide for ultracapacitors*, Carbon (2010) 48, 7, 2118-2122

[21] Zhu Y., Murali S., Stoller M. D., Ganesh K. J., Cai W., Ferreira P. J., Pirkle A., Wallace R. M., Cychosz K. A., Thommes M., Su D., Stach E. A., Ruoff R. S., *Carbon-Based Supercapacitors Produced by Activation of Graphene*, Science (2011) 332, 1537-1541

[22] Zhang L. L., Zhao X., Stoller M. D., Zhu Y., Ji H., Murali S., Wu Y., Perales S., Clevenger B., Ruoff R. S., *Highly Conductive and porous Activated Reduced Graphene Oxide Films for High-Power Supercapacitors*, Nano Letters (2012) 12, 1806-1812

[23] Kim T., Jung G., Yo S., Suh K. S., Ruoff R. S., *Activated Graphene-Based Carbons as Supercapacitors electrodes with Macro- and Mesopores*, (2013) 7, 8, 6899-6905

[24] Sugimoto, W., Iwata H., Yasunaga Y., Murakami Y., Takasu Y., *Preparation of ruthenic acid nanosheets and utilization of its interlayer surface for electrochemical energy storage*, Angewante Chemical International Edition (2003) 42 4092-4096

[25] Kim H., Popov B. N., *Characterization of hydrous ruthenium oxide/carbon nanocomposite supercapacitors prepared by a colloidal method*, (2002) 104, 1, 52-61

[26] Chen W., Rakhi R. B., Hu L., Xie X., Cui Y., Alshareef H. N., *High-Performance Nanostructured Supercapacitors on a Sponge*, Nano Letters (2011) 11, 5165-5172

[27] Lee J. Y., Liang K., An H., Lee Y. H., *Nickel oxide/carbon nanotubes nanocomposite for electrochemical capacitance*, Synthetic Metals (2005) 150, 153-157

[28] Zhang Y., Sun X., Pan L., Li H., Sun Z., Sun C., Tay B. K., *carbon nanotube-ZnO nanocomposite electrodes for supercapacitors*, (2009) 180, 1525-1528

[29] Chen Y., Zhang X., Zhang D., Yu P., Ma Y., *High performance supercapacitors based on reduced graphene oxide in aqueous and ionic liquid electrolytes*, (2011) 49, 2, 573-580

[30] Zhou C., zhang Y., Li Y., Liu j., *Construction of High-Capacitance 3D CoO-Polypyrrole Nanowire Array Electrode for Aqueous Asymmetric Supercapacitor*, Nano Letters (2013) 13, 2078-2085

[31] Amatucci G. G., Badway F., Du Pasquier A., Zheng T., *An Asymmetric Hybrid Nonaqueous Energy Storage Cell*, Journal of The Electrochemical Society (2001) 148, 8, A930-A939

[32] Naoi K., Naoi W., Aoyagi S., Miyamoto J.-I., Kamino T., *New Generation « Nanohybrid Supercapacitor »*, Accounts of chemical research (2013) 46, 5, 1075-1083

[33] Karthikeyan K., Aravindan V., Lee S. B., Jang I. C., Lim H. H., Park G. J., Yoshio M., Lee Y. S., *A novel asymmetric hybrid supercapacitor based on Li_2FeSiO_4 and activated carbon electrodes*, Journal Alloys and Compounds (2010) 504, 1, 224-227

[34] Karthikeyan K., Aravindan V., Lee S. B., Jang I. C., Lim H. H., Park G. J., Yoshio M., Lee Y. S., *Electrochemical performance of carbon-coated lithium manganese silicate for asymmetric hybrid supercapacitors*, Journal of Power Sources (2010) 195, 11, 3761-3764

[35] Naoi K., Nagano Y., *Li-ion Hybrid Supercapacitors in Organic Medium*, (2013) Wiley-VCH BOOK

[36] Honda Y., Haramoto T., Takeshige M., Shiozaki H., Kitamura T., Ishikawa M., *Aligned MWCNT Sheet Electrodes Prepared by Transfer Methodology Providing High-Power Capacitor Performance*, Electrochemical and Solid-State Letters (2007) 10, 4, A106-A110

[37] Abbas Q., Pajak D., Frackowiak E., Beguin F., *Effect of binder on the performance of carbon/carbon symmetric capacitors in salt aqueous electrolyte*, Electrochemical Acta (2014) 140, 132-138

[38] Honda Y., Takeshige M., Shiozaki H., Kitamura T., Ishikawa M., *Excellent Frequency Response of vertically Aligned MWCNT Electrode for EDLC*, Electrochemistry (2007) 8, 586-588

[39] Futaba D. N., Hata K., Yamada T., Hiraoka T., Hayamizu Y., Kakudate Y., Tanaike O., Hatori H., Yumura M., Iijima S., *Shape-engineerable and highly densely packed single-walled carbon nanotubes and their application as super-capacitor electrodes*, Nature Materials (2006) 5, 987-994

[40] Zhang H., Cao G., Yang Y., Gu Z., *Comparison Between Electrochemical Properties of Aligned Carbon Nanotube Array and Entangled Carbon Nanotube Electrodes*, Journal of The Electrochemical Society (2008) 155, 2, K19-K22

[41] Basirico L., Lanzara G., *Moving towards high-power high-frequency and low-resistance CNT supercapacitors by tuning the CNT length, axial deformation and contact resistance*, Nanotechnology (2012) 23, 305401

[42] Lin J., zhang C., Yan Z., Zhu Y., Peng Z., Hauge R. H., Natelson D., Tour J. M., *3-Dimensional Graphene Carbon Nanotube Carpet-Based Microsupercapacitors with High electrochemical Performance*, Nano Letters (2012) 13, 72-78

[43] J. R. Miller, R. A. Outlaw, B. C. Holloway. *Graphene Double-Layer Capacitor with ac Line-Filtering Performance*. Science 329, 1637 (2010)

[44] Cai M., Outlaw R. A., Quinlan R. A., Premathilake D., Butler S. M., Miller J. R., *Fast Response, Vertically Oriented Graphene Nanosheet Electric Double Layer Capacitors Synthesized from C_2H_2*, ACS Nano (2014) 8, 6, 5873-5882

[45] K. Sheng, Y. Sun, C. Li, W. Yuan, G. Shi. *Ultrahigh-rate supercapacitors based on electrochemically reduced graphene oxide for ac line-filtering*, Scientific Reports (2011) 2 247

[46] Lukatskaya M., Mashtalir O., Ren C., Dall'Agnese Y., Rozier P., Taberna P., Naguib M., Simon P., Barsoum M., Gogotsi Y., *Cation Intercaltion and High Volumetric capacitance of Two-Dimensional Titanium Carbide*, Science (2013) 341, 1502-1505

[47] P.L. Taberna, C. Portet, P. Simon. *Electrode surface treatment and electrochemical impedance spectroscopy study on carbon/carbon supercapacitors*, Applied Physics A (2006) 82, 639-646

[48] E. Frackowiak. *Carbon materials for supercapacitor application*, Physical Chemistry Chemistry Physics (2007) 9, 1774-1785

[49] T. M. Dinh, K. Armstrong, D. Guay, D. Pech. *High-resolution on-chip supercapacitors with ultra-high scan rate ability*. Journal of Materials Chemistry A (2014) 2, 7170-7174

[50] S. Ramesh, L. M. Ericson, V. A. Davis, R. K. Saini, C. Kittrell, M. Pasquali, W. E. Billups, W. W. Adams, R. H. Hauge, R. E. Smalley. *Dissolution of Pristine Single Walled Carbon Nanotubes in Superacids by Direct Protonation.* J. Phys Chem. B, 108, 8794 (2004)

[51] D. S Hecht, A. M. Heintz, R. Lee, L. Hu, B. Moore, C. Cucksey, S. Risser. *High conductivity transparent carbon nanotube films deposited from superacid.* Nanotechnology, 22, 075201 (2011)

[52] N. Behabtu, J. R. Lomeda, M. J. Green, A. L. Higginbotham, A. Sinitskii, D. V. Kosynkin, D. Tsentalovich, A. N. G. Parra-Vasquez, J. Schmidt, E. Kesselman, Y. Cohen, Y. Talmon, J. M. Tour, M. Pasquali. *Spontaneous high-concentration dispersions and liquid crystals of graphene. Nature Nanotech., 5, 406 (2010)*

[53] V. A. Davis, A. N. G. Parra-Vasquez, M. J. Green, P. K. Rai, N. Behabtu, V. Prieto, R. D. Booker, J. Schmidt, E. Kesselman, W. Zhou, H. Fan, W. W. Adams, R. H. Hauge, J. E. Fischer, Y. Cohen, Y. Talmon, R. E. Smalley, M. Pasquali. *True solutions of single-walled carbon nanotubes for assembly into macroscopic materials.* Nature Nanotech., 4, 830 (2009)

[54] M.D. Stoller, R.S. Ruoff. *Best practice methods for determining an electrode material's performance for ultracapacitors.* Energy & Environmental Science (2010) 3, 1294-1301

[55] C Portet, P.L Taberna, P Simon, C Laberty-Robert. *Modification of Al current collector surface by sol–gel deposit for carbon–carbon supercapacitor application.* Electrochimica Acta (2004) 49, 905-912

[56] P. Huanga, M. Heone, D. Pecha, M. Bruneta, P.-L. Tabernac, Y. Gogotsi, S. Loflandf, J. D. Hettingerf, P. Simon. *Micro-supercapacitors from carbide derived carbon (CDC) films on silicon chips.* Journal of Power Sources (2013) 225, 240-244

[57] C. Du, N. Pan. *Supercapacitors using carbon nanotubes films by electrophoretic deposition.* Journal of Power Sources (2006) 160, 1487-1494

[58] D. Pech, M. Brunet, H. Durou, P. Huang, V. Mochalin, Y. Gogotsi, P.-L. Taberna, P. Simon. *Ultrahigh-power micrometre-sized supercapacitors based on onion-like carbon.* Nature Nanotechnology (2010) 5, 651-654

[59] R. Lin, P. L. Taberna, J. Chmiola, D. Guay, Y. Gogotsi, P. Simon. *Microelectrode Study of Pore Size, Ion Size, and Solvent Effects on the Charge/Discharge Behavior of Microporous Carbons for Electrical Double-Layer Capacitors.* Journal of The Electrochemical Society (2009) 156, A7-A12

[60] N. Sano, H. Wang, M. Chhowalla, I. Alexandrou, G. A. J. Amaratunga. *Nanotechnology: Synthesis of carbon 'onions' in water.* Nature (2001) 414, 506-507

[61] X. Zhao, B. Chu, B. Ballesteros, W. Wang, C. Johnston, J. M. Sykes, P. S. Grant. *Spray deposition of steam treated and functionalized single-walled and multi-walled carbon nanotube films for supercapacitors.* Nanotechnology (2009) 20, 065605

[62] Sundaresan R., Burk D., Fossum J., *Potential improvement of polysilicon solar cells by grain boundary and intragrain diffusion of aluminum*. J. Applied Physics 55, 1162 (1984)

[63] M. Cai, R. A. Outlaw, S. M. Butler, J. R. Miller, *A high density of vertically-oriented graphenes for use in electric double layer capacitors*. Carbon 50, 5481 (2012)

[64] Y. Li, K. Sheng, W. Yuan, G. Shi, *A high-performance flexible fibre-shaped electrochemical capacitor based on electrochemically reduced graphene oxide.* Chemical Communications 49, 291 (2013)

[65] P. Kossyrev. *Carbon black supercapacitors employing thin electrodes.* Journal of Power Sources 201, 347 (2012)

[66] Chai Y., Javey A., Wong H., *Low-Resistance Electrical Contact to Carbon Nanotubes With Graphitic Interfacial Layer*. IEEE Transaction on Electron Devices (2012) 59, 1

[67] Lee J., Yoo K., *Formation of low-resistance ohmic contacts between carbon nanotube and metal electrodes by a rapid thermal annealing method*, Journal of Physics D: Applied Physics (2000) 33, 1953-1956

[68] Wu W., Hu A., Li X., Wei J. Q., Shu Q., Wang K. L., Yavuz M., Zhou Y. N.. *Vacuum brazing of carbon nanotube bundles*, Materials Letters (2008) 4486-4488

[69] Yan J., Zou G., Wu A., Ren J., Yan J., Hu ., Liu L., Zhou Y. N.. *Effect of PVP on the low temperature bonding process using polyol prepared Ag nanoparticle paste for electronic packaging application, Journal of Physics:* Conference Series (2012) 379, 012024